

**Synthesis and characterization of ferrite
nanoparticles/superconductor composites**

Sumayyah Naeem

41-FBAS/MS-PHY/F10

A thesis submitted in partial fulfillment
of the requirement for the degree of

MASTER OF PHILOSOPHY

in

PHYSICS



DEPARTMENT OF PHYSICS

INTERNATIONAL ISLAMIC UNIVERSITY ISLAMABAD

2012



Accession No TH-9359

MS
530.41
SUS

- 1 Ferrite composites
- 2 Superconducting nanoparticles

بِسْمِ اللَّهِ الرَّحْمَنِ الرَّحِيمِ

In the Name of Allāh, the Most Gracious, the Most Merciful

Dedicated to

My Ammi

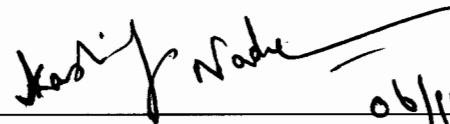
&

Me

FORWARDING SHEET BY RESEARCH SUPERVISOR

The thesis entitled "Synthesis and characterization of ferrite nanoparticles/superconductor composites" submitted by Sumayyah Naeem in partial fulfilment of MS degree in Physics has been completed under my guidance and supervision. I am satisfied with the quality of student's research work and allow him to submit this thesis for further process to graduate with Master of Science Degree from Department of Physics, as per IIU rules & regulation.

Date: _____


06/11/12

Dr. Kashif Nadeem

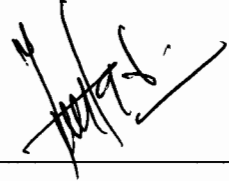
(Supervisor)

Assistant Professor

Department of Physics

International Islamic University

Islamabad.



Dr. Muhammad Mumtaz

(Co-supervisor)

Assistant Professor (TTS)

Department of Physics

International Islamic University

Islamabad.


ACCEPTANCE BY THE VIVA VOCE COMMITTEE

Title of Thesis: “Synthesis and Characterization of ferrite nanoparticles/superconductor composites”
Name of Student: Sumayyah Naem
Registration No. 41-FBAS/MSPHY/F10

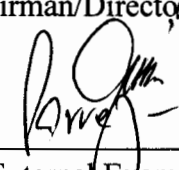
Accepted by the Department of Physics, Faculty of Basic & Applied Sciences, INTERNATIONAL ISLAMIC UNIVERSITY ISLAMABAD, in partial fulfilment of the requirements for the Master of Science in Physics with specialization in Nanotechnology.

VIVA VOCE COMMITTEE

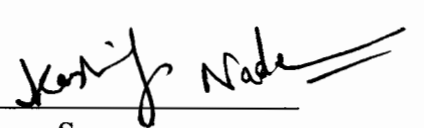
Dr. Shaista Shahzad
Chairperson
Department of Physics (FC, FBAS)
International Islamic University
Islamabad



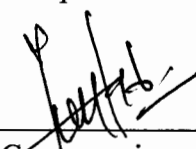
Chairman/Director/Head



External Examiner



Supervisor



Co-supervisor

Dated:
22/10/2012

ACKNOWLEDGEMENT

All praise for Almighty Allah, the creator of the universe with its mysteries of logic, who is our benefactor. His revolutions are source of knowledge and He invites us to unravel the secrets of nature.

All respects for His Holy Prophet Hazrat Muhammad (PBUH) who is forever an ivory tower for all of us.

I am grateful to my immediate supervisor **Dr. Kashif Nadeem**, Assistant Professor of Physics, Department of Physics, IIU, Islamabad for his countless support, invaluable guidance, skilled advice, elaborate instruction and benevolent attitude in completion of my research work and thesis.

I wish to express my gratitude to my co-supervisor **Dr. Muhammad Mumtaz**, Assistant Professor of Physics, Department of Physics, IIU, Islamabad for flourishing all the possible facilities to carry out this research work.

I am grateful to **Dr. Nawazish Ali Khan** and his all students of Material Science Laboratory, Deptt. of Physics, QAU, Islamabad for their cooperation.

I am thankful to my chairperson **Dr. Shaista Shahzada**, Assistant Professor of Physics, Department of Physics, IIU, Islamabad for her kind and loving support.

Last but not the least I would like to pay gratitude to my loving mother, sisters specially Farah and Sumera and brothers whose affections and encouragement brightened my academic career.

SumayyahNacem

TABLE OF CONTENT

1: Introduction	1
1.1 Superconductivity	1
1.2 Classification of superconductor	4
1.2.1 Type I superconductor	5
1.2.2 Type II superconductor	6
1.3 Critical parameters	7
1.3.1 Critical temperature (T_c)	7
1.3.2 Critical current density (J_c)	7
1.3.3 Critical magnetic field (H_c)	8
1.4 BCS theory	9
1.5 Copper thallium (CuTl) based superconductor	10
1.6 Nanotechnology	13
1.7 Nanoparticles	15
1.8 Nanoparticles/Superconductor composites	17
1.9 Motivation	17
2: Review of Literature	19
3: Synthesis and Experimental Techniques	24
3.1 Synthesis of superconductors	24
3.2 Synthesis of nanoparticles	24
3.2.1 Top down approach	25
3.2.2 Bottom up approach	26

3.3 Synthesis of nanoparticles/superconductor composites	26
3.4 Experimental techniques	31
3.4.1 X-ray diffraction	31
3.4.2 Scanning electron microscopy	33
3.4.3 Energy Dispersive X-ray analysis	34
3.4.4 Fourier transforms infrared spectroscopy	36
3.4.5 Resistivity measurements	37
3.4.6 AC susceptibility measurements	38
4: Results and Discussion	41
4.1 X-ray diffraction (XRD)	43
4.2 Scanning electron microscopy (SEM)	46
4.3 Fourier transforms infrared spectroscopy(FTIR)	48
4.4 Resistivity measurements	52
4.5 AC susceptibility measurements	54
4.6 Conclusion	57
References	59

LIST OF FIGURES

1: Introduction	1
Fig. 1.1: (a) Extinct of electrical resistivity (b) demonstration of Meissner effect	2
Fig. 1.2: Transition temperature progress vs. year	4
Fig. 1.3: Type-I superconductor	5
Fig. 1.4: Type-II superconductor	6
Fig. 1.5: Demonstration of critical temperature (T_c)	7
Fig. 1.6: I-V Characteristic of a superconductor	7
Fig. 1.7: Dependence of different states of superconductor on magnetic field and temperature	8
Fig. 1.8: Representation of Cooper pair	9
Fig. 1.9: (a) General crystal structure of high temperature superconductor	11
Fig. 1.9: (b) CuTl-1223 unit cell crystal structure	11
Fig. 1.10: Representation of size comparison (1 m to 0.1 nm)	13
Fig. 1.11: SEM of gold nanoparticles	14
Fig. 1.12: Nanotechnology in different fields	15
3: Synthesis and Experimental Techniques	23
Fig. 3.1: Top down and bottom up approach to synthesize the nanoparticles	25
Fig. 3.2: Schematic diagram of $Cu_{0.5}Tl_{0.5}Ba_2Ca_2Cu_3O_{10-\delta}$ superconductor	27
Fig. 3.3: Synthesis diagram of $ZnFe_2O_4$ nanoparticles	28
Fig. 3.4: Synthesis diagram of nanoparticles/ superconductor composites	30

Fig. 3.5: Diffraction of X-rays	31
Fig. 3.6: X-ray diffraction scheme	32
Fig. 3.7: SEM schematic diagram	34
Fig. 3.8: EDX spectrum	35
Fig. 3.9: Michelson interferometer schematically	36
Fig. 3.10: Resistivity setup	37
Fig. 3.11: AC-susceptibility phase diagram	39
Fig. 3.12: AC susceptibility setup	40
4: Results and Discussion	41
Fig. 4.1: The XRD scan of $ZnFe_2O_4$ nanoparticles	44
Fig. 4.2: XRD pattern of nanoparticles/superconductor composites	45
Fig. 4.3: (a) SEM micrograph of $Cu_{0.5}Tl_{0.5}Ba_2Ca_2Cu_3O_{10-\delta}$ superconductor	46
Fig. 4.3: (b) SEM image of nanoparticles/superconductor composites	46
Fig. 4.4: EDX image of $Cu_{0.5}Tl_{0.5}Ba_2Ca_2Cu_3O_{10-\delta}$ superconductor	47
Fig. 4.5: FTIR spectrum of $ZnFe_2O_4$ nanoparticles	49
Fig. 4.6: (A) FTIR spectra of nanoparticles/superconductor composites	50
Fig. 4.6: (B) FTIR spectra of nanoparticles/superconductor composites	51
Fig. 4.7: (a) Resistivity vs. temperature measurements of nanoparticles/ superconductor composites	53
Fig. 4.7: (b) Resistivity vs. temperature measurements of nanoparticles/ superconductor composites	53
Fig. 4.8: The critical temperature vs. $ZnFe_2O_4$ -content of nanoparticles/ superconductor composites	54
Fig. 4.9: The AC-susceptibility vs. temperature measurements of nanoparticles/superconductor composites	55

LIST OF TABLES

4: Results and Discussion	41
Table 4.1: Quantitative analysis of elements of Fig. 4.4	48

DECLARATION

I *Sumayyah Naeem* (41-FBAS/MSPHY/F10), student of MS Physics (session 2010-2012) hereby declared that the matter printed in the thesis titled “**Synthesis and characterization of ferrite nanoparticles/superconductor composites**” is my own work and has not been published or submitted as research work or thesis in any form in any other University or Institute in Pakistan or abroad.

Dated: _____

Signature of Deponent

ABSTRACT

The $(ZnFe_2O_4)_y / (Cu_{0.5}Tl_{0.5})Ba_2Ca_2Cu_3O_{10-\delta}$ ($y = 0, 0.05, 0.1, 0.15, 0.2, 0.25, 0.5, 1,$ and 2%) nanoparticles/superconductor composites has been synthesized by the solid-state reaction method at 860°C . The $ZnFe_2O_4$ nanoparticles have been separately synthesized by sol-gel method at 900°C . The structural and physical properties have been examined by X-ray diffraction (XRD), Scanning electron microscopy (SEM), Fourier transforms infrared (FTIR) spectroscopy, Resistivity, and AC susceptibility techniques. X-ray diffraction of $Cu_{0.5}Tl_{0.5}Ba_2Ca_2Cu_3O_{10-\delta}$ superconductor matrix exhibits the tetragonal structure and shows the CuTl-1223 as a dominant phase with small presences of CuTl - 1234 phases in these samples. There is no significant change observed in lattice parameters with increasing the concentration of nanoparticles in CuTl-1223 superconductor and the structure of these composites remain tetragonal. The SEM proofs the intergranular structure of the host CuTl- 1223 superconducting matrix. The FTIR spectrum of Zn ferrite nanoparticles reveals the existence of vibrational bonds (420 and 546 cm^{-1}) which are specific for ferrite spinel structure. The FTIR measurements also revealed the inclusion of $ZnFe_2O_4$ nanoparticles in these composites. The zero resistivity critical temperature [T_c ($R=0$)] is found to decrease with increase the concentration of $ZnFe_2O_4$ nanoparticles due to poor grain connectivity and lowest porosity. The AC susceptibility measurements of composites exhibit the decrease in magnitude of diamagnetism due to ferrimagnetic behavior of Zn ferrite nanoparticles.

Chapter # 1

Introduction

The appearance of superconductor, nanotechnology and their composites is a leap forward for science, a countless set back to unawareness, a big bang of enlightenment; a practical awareness of the principles; a reform effort the fruits of which will give advantage to every application. Superconductive phenomena created the worldwide excitements than the others [1]. Superconductors and nanotechnology have a bright scientific and practical future in the emerging field of physics which causes a vicissitude in the scientific world. Now both fields are generating new materials and devices with wide applications. This chapter contains precious information about superconductors, its brief history, classification, and describe the hidden mysteries of nanotechnology [2, 3].

1.1 Superconductivity

Superconductivity is a phenomenon in which electrical resistivity of materials drops suddenly to zero at critical transition temperature (T_c). The elements like *Sn*, *Pb*, *Nb* etc. and some natural materials such as *MgB₂* and Lithium (Li) have shown higher critical temperature of 40 K and 20 K respectively [4-6]. Superconductor comprises the following two characteristics as shown in Fig. 1.1 (a, b).

- (a) below critical temperature, extinct the electrical resistivity [7, 8],
- (b) below a critical magnetic field, expel external magnet field [9].

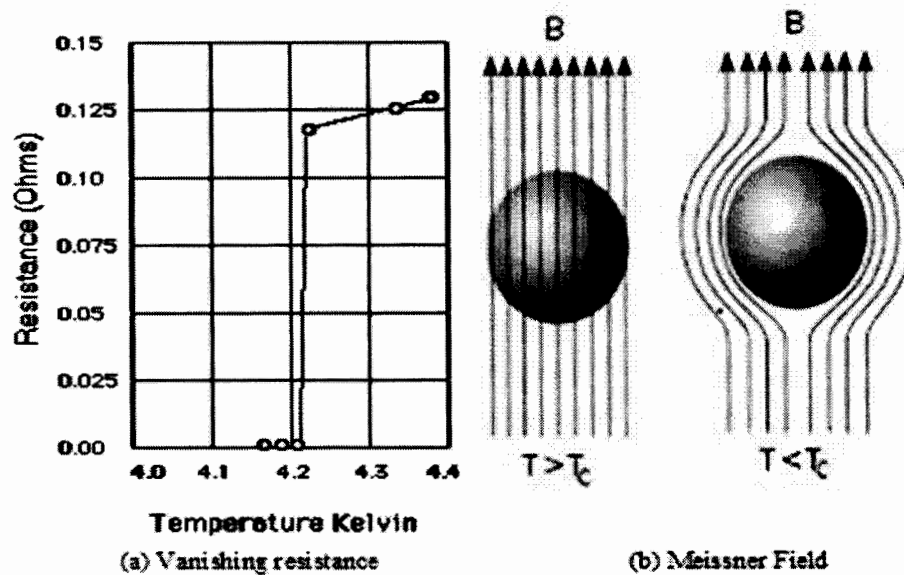


Fig. 1.1: (a) Vanishing of electrical resistivity at T_c (b) demonstration of Meissner effect [1, 9].

Superconductivity was first discovered by a Dutch Physicist H. Kamerlingh Onnes in 1911 [10]. He found that at 4 K temperature, the resistance of solid mercury abruptly dropped to zero. It was obvious that the specimen undergoes a phase transition from normal electrical resistivity and this phenomenon is known as superconductivity [11]. In 1913 superconductivity of lead and niobium nitride was obtained at 7 and 16 K, respectively [12]. After that Meissner and Ochsenfeld (1933) studied the effect of magnetic field on superconductivity, they found that material completely repel the magnetic field lines (B) when its temperature reduces below the critical temperature and is known as Meissner effect [9].

Two brothers H. London and F. London developed a microscopic superconductivity theory in 1935 which is also known as London theory. This theory was followed by two fluid model of Gorter and Casimir and electromagnetic theories of

London brothers [13]. In 1950, superconductor responsibility came with Froehlich's theoretical model and the first electron-phonon interaction and isotopic effect came under discussion [14]. In 1957 J. Barden, L. Coopers and J. R. Schrieffer successfully described the nature of superconductors and this theory is known as BCS Theory [15]. Superconductivity in oxides was discovered in 1986 by Bednorz and Muller in high temperature superconductor *La-Ba-Cu-O* (LBCO) at 30 K [16, 17]. After this in 1987, C. W. Chu and his colleagues discovered the new oxide superconductor *Y-Ba-Cu-O* with 90 K critical temperature [18]. In 1988, $Bi_2Sr_2Ca_{n-1}Cu_nO_{2n+4}$ (BSCCO) family was discovered with maximum transition temperature up to 110 K [19-21]. *Tl-Sr-Ca-Cu-O* system discovered with 115 K T_c and after this several new phases have been prepared e.g. $Tl_mBa_2Ca_{n-1}Cu_nO_{2n+2}$ [22-24]. The high critical temperature attained by $Cu_{1-x}Tl_xBa_2Ca_2Cu_3O_{10-\delta}$ ($Cu_{1-x}Tl_x-1223$) superconductor also attains the attention of scientific community [25]. A fascinating family of iron pnictide/chalcogenide layer of *anti-PbO* structure superconductors discovered with a critical temperature up to 50 K. Figure 1.2 represents the rapid change of T_c of superconductors with the passage of time.

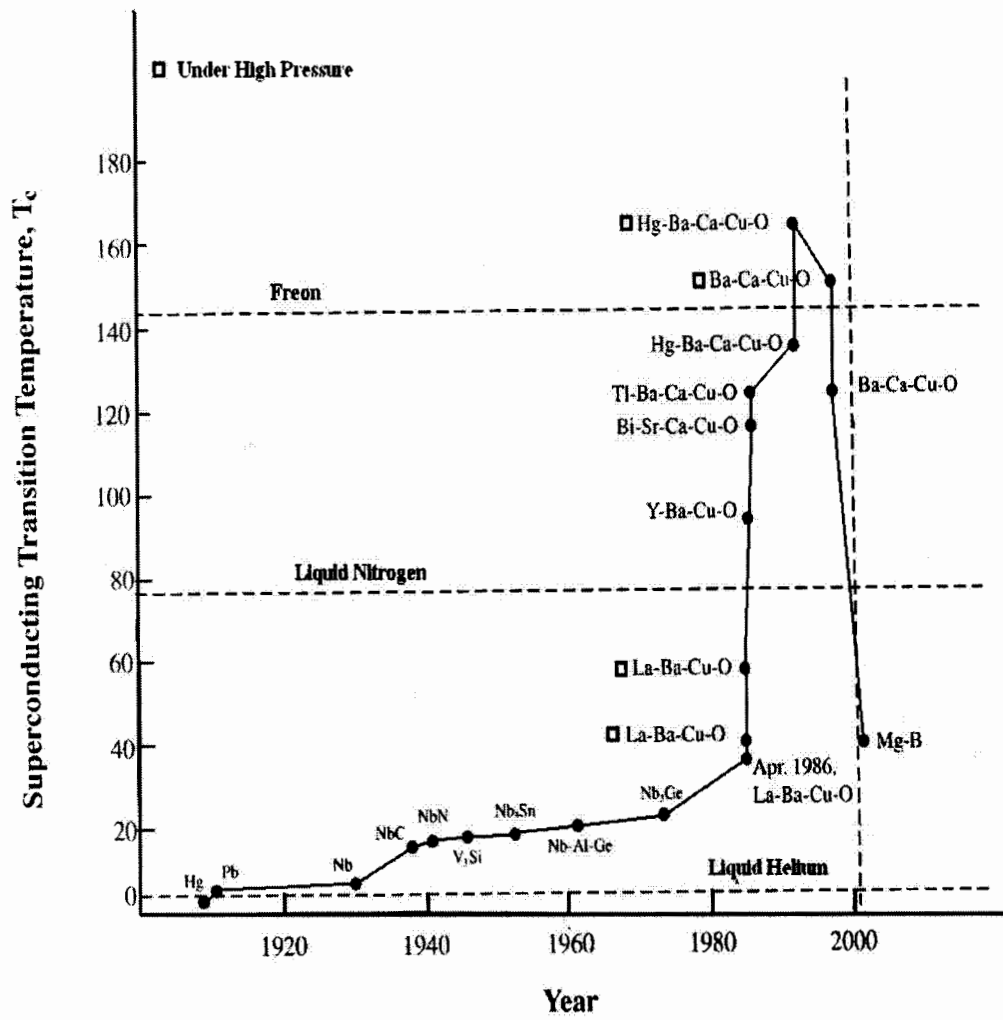


Fig. 1.2: Transition temperature progressvs. year [26].

1.2 Types of superconductors

According to their magnetic properties, superconductor can be divided into two following types:

1.2.1 Type-I superconductors

Type I superconductors are pure metals e.g. lead, mercury and tin etc. Meissner effect is applicable to Type I superconductors. Figure 1.3 explains the dependence of induced magnetic field on applied magnetic field for Type 1 superconductor. Induced magnetic field exactly cancels the applied magnetic field until there is an abrupt change from superconducting state to normal state. Due to zero magnetic field inside the superconductor, they show the immaculate diamagnetism. These are also called soft superconductor [27].

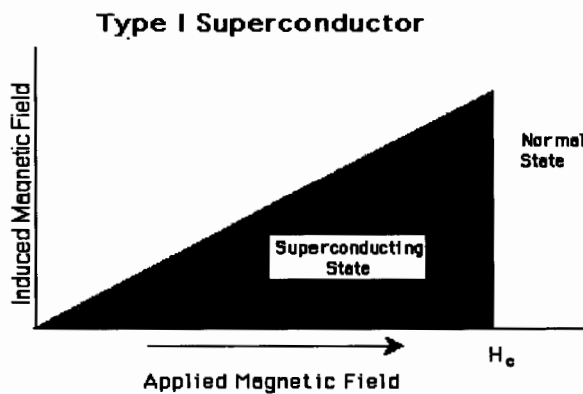


Fig. 1.3: Type-I superconductor [27].

The value of critical field H_c is quite low for these superconductors. This is the main disadvantage of Type I superconductor in practical applications because they cannot carry high currents.

1.2.2 Type-II superconductors

Type II superconductors are high temperature ceramic superconductors such as $YBa_2Cu_3O_7$ (YBCO) and $Bi_2CaSr_2Cu_2O_9$. Figure 1.4 graph exhibits the induced magnetic field versus applied field for Type II superconductor.

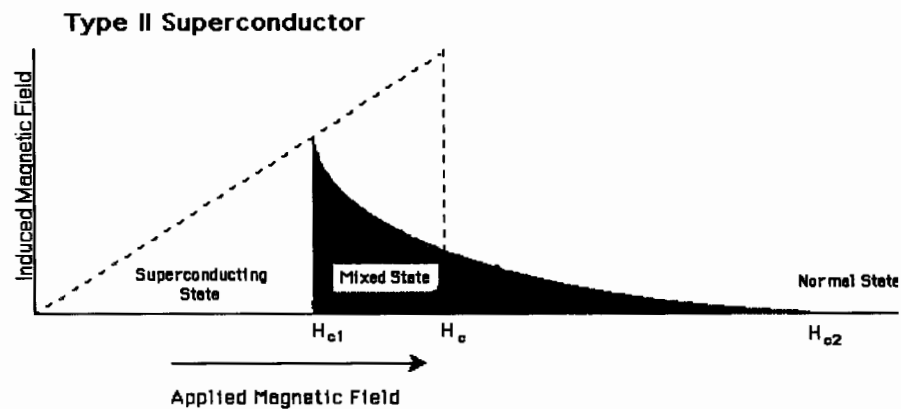


Fig. 1.4: Type-II superconductor [27].

There are two critical fields H_{c1} and H_{c2} in Type II superconductor. Under H_{c1} the magnetic lines are completely excluded and show the negative magnetization. At this stage material exhibits a perfect diamagnetic behavior. While between H_{c1} and H_{c2} the magnetic lines are partially penetrate into the material and exhibit the partially diamagnetic behavior. The state between H_{c1} and H_{c2} fields in superconductors is said to be in vortex state or mixed state. Beyond H_{c2} , they become paramagnetic with small positive magnetization and behave as a normal material. Type II superconductors properties are observed above the field H_{c2} . Incomplete Meissner effect can be studied between lower and upper critical field where the flux density $B=0$. Type II superconductor are also known as hard superconductors [28].

1.3 Critical parameters of superconductors

A transition can occur from superconducting state back to its normal state by three ways such as; Critical temperature T_c , critical current density J_c and critical magnetic field H_c .

1.3.1 Critical temperature (T_c)

The temperature at which material cooled below room temperature and exhibits the zero resistivity is known as its critical temperature (T_c) as demonstrated in Fig. 1.5 [29].

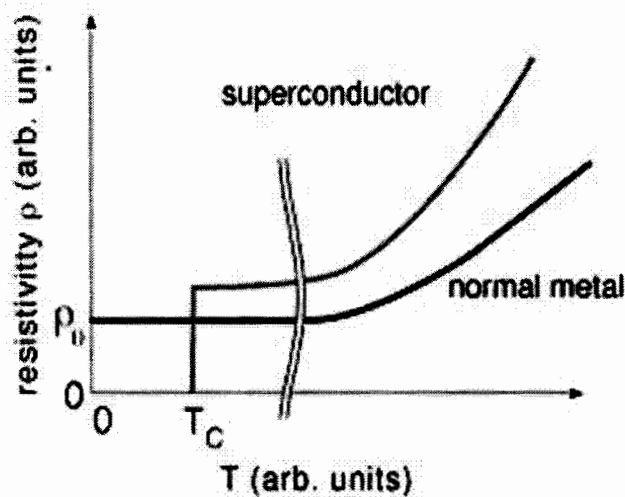


Fig. 1.5: Demonstration of critical temperature (T_c) [29].

1.3.2 Critical current density (J_c)

The phenomenon in which superconductor can carry maximum current is known as critical current density (J_c). For practical applications J value should be $1000\text{A}/\text{mm}^2$

[30]. The demonstration of the critical current density (J_c) is shown in Fig. 1.6 at low temperature.

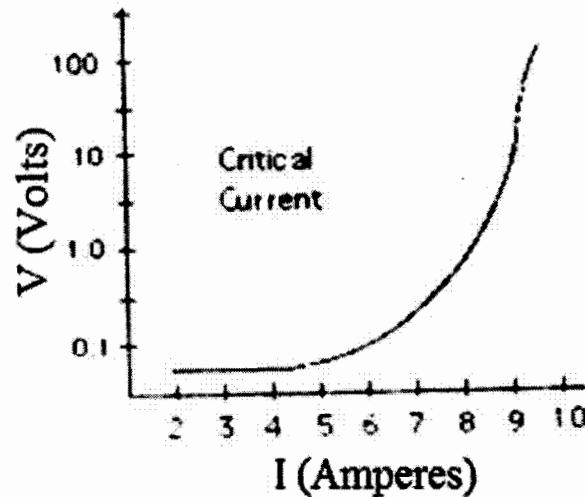


Fig. 1.6: I-V Characteristic of a superconductor [30].

1.3.3 Critical magnetic field (H_c)

The maximum magnetic field value at which the superconductor goes to normal resistive state at a given temperature is known as its critical magnetic field (H_c). A specific region of temperature and magnetic field exist in all superconductors, in which a material gets the superconducting behavior. The material attains the normal state outside the superconducting region on the application of specific magnetic field at particular temperature as shown in the Fig. 1.7 [31].

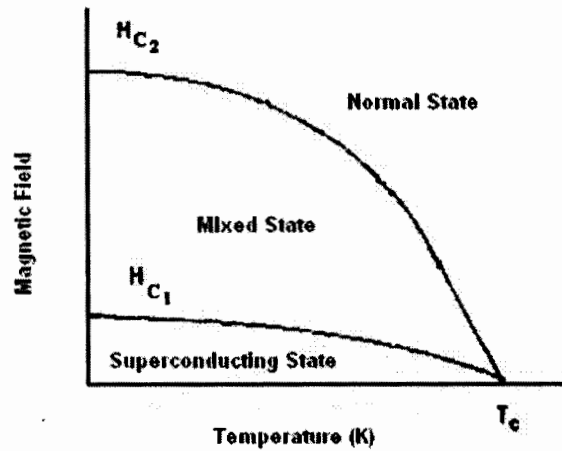


Fig. 1.7: Dependence of different states of superconductor on magnetic field and temperature [32].

1.4 BCS Theory

The quantum mechanical explanation of superconductivity was explained by three scientists Bardeen, Cooper and Schrieffer in 1957 and is known by BCS theory. Figure 1.8 shows that superconducting behavior appeared to be that of electrons by means of interchange of phonons and formed +ve and -ve region.

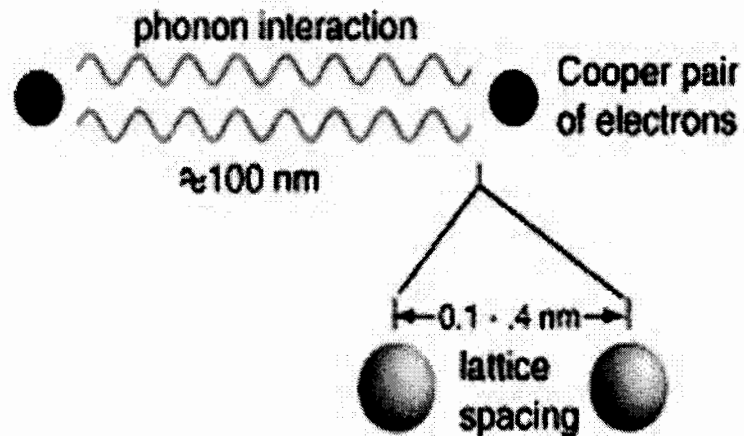


Fig. 1.8: Representation of Cooper pair [33].

Due to this electron pair is pull together and push apart without a collision and formed an electron pair which is known as Cooper pair [31]. The collection of all particles under critical temperature in the minimum energy level is called as Boson condensation in which all the particles have same wavefunction [11]. So according to BCS theory, superconductivity can be explained as condensate of Cooper pair seemed at $T < T_c$. It represent that the free electric current is carried by Cooper pair. The distance to which Cooper pair keeps its coupled motion among the lattice point in a superconductor is called its coherence length (ξ). The shortest distance at which superconductivity may be usually established is 10^{-6} m [34].

1.5 Copper Thallium (CuTl) based superconductor

CuTl based superconductors are one of the interesting high- T_c superconductors having many practical applications. Figure 1.9 (a) shows the general structure of high temperature superconductor. CuTl based superconductors are designed by the Cu based $CuBa_2Ca_{n-1}Cu_nO_{2n+2}[Cu-12(n-1)n$ (where $n = 1, 2, 3, \dots$)] superconductors which consist of tetragonal structure [35]. Among all the Cu based superconductor families the Cu-1223 superconductor has the highest critical temperature 120 K [36-39]. The ratio of ab-plane coherence length and c-axis coherence length is known as the anisotropy ($\gamma = \xi_{ab} / \xi_c$). The least anisotropic property of this compound is ($\gamma = 1.6$) and have long c-axis coherence length [40-41]. It is not simple to synthesize this compound at higher pressure but Thallium (Tl) addition into charge reservoir layer make it simple to obtain a superconducting state. In this procedure “Tl” behaves as structure stabilizer.

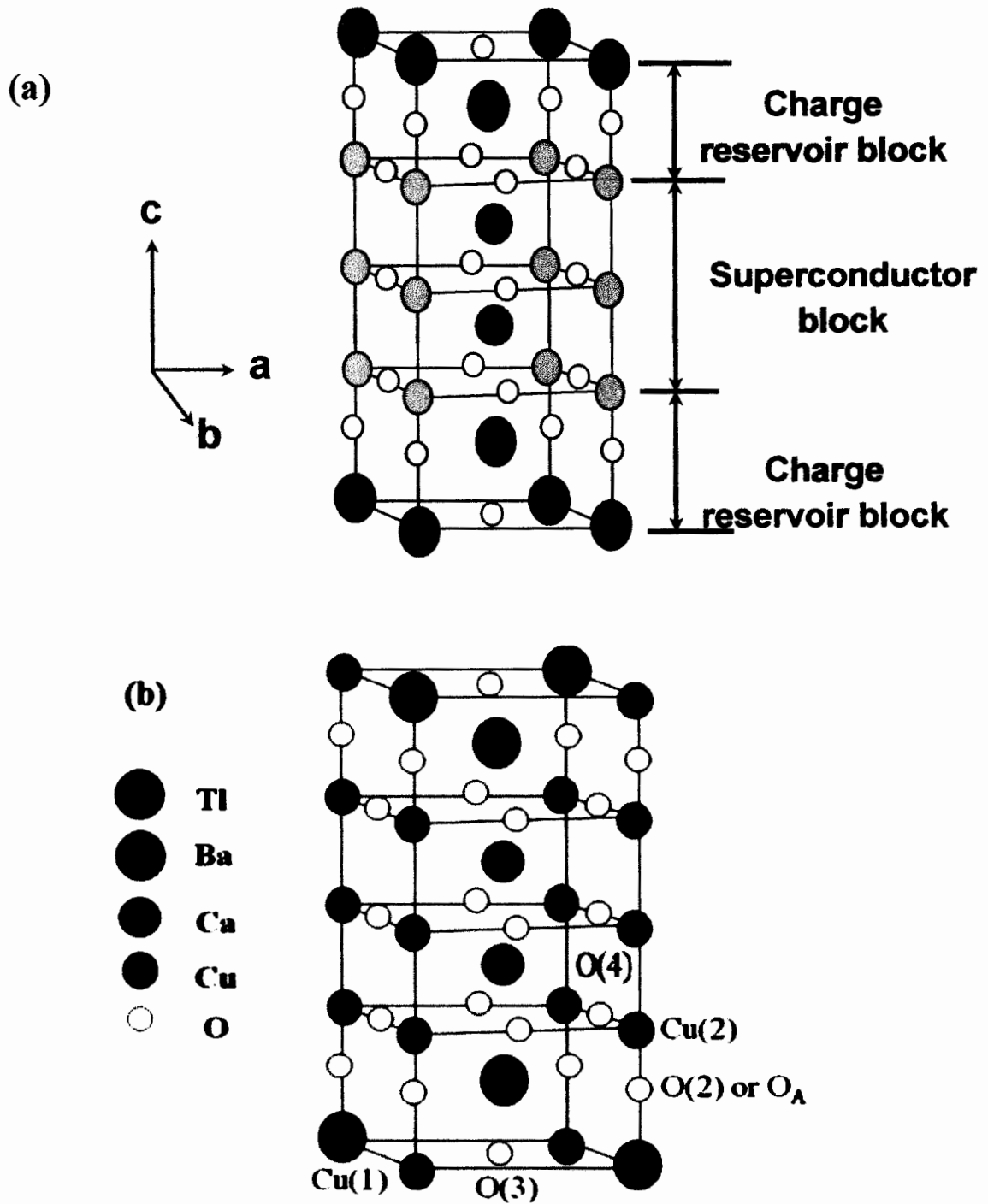


Fig. 1.9: (a) General crystal structure of high temperature superconductor [46], (b) CuTl-1223 unit cell crystal structure [47].

The induction of Tl in $[Cu-12(n-1)n]$ compound introduced a new subfamily of $Cu_{1-x}Tl_x 12(n-1)n$ which is the close derivative of this compound [42-44]. The superconductor $Cu_{1-x}Tl_x Ba_2 Ca_2 Cu_3 O_{10-\delta}$ ($Cu_{1-x}Tl_x-1223$) has the highest critical temperature ($T_c = 130$ K). $Cu_{1-x}Tl_x Ba_2 O_{4n-\delta}$ is the semi insulating charge reservoir layer that smoothly increase the anisotropy ($\gamma=5$) of this superconductor family [25, 45].

Figure 1.9 (b) shows the unit cell of CuTl-1223 superconductor in which $Cu_{1-x}Tl_x Ba_2 O_{4-\delta}$ acts as a charge reservoir and CuO_2 three planes which is separated by two Ca atoms in unit cell. The Ba atoms used to connect the superconducting CuO_2 planes with each other in unit cell are pyramid type is called p-plane. The central plane or s-plane is sandwiched plane between the p-planes which is connected by Ca atoms with the outer planes. Due to carrier p-planes are over doped whereas optimally doped planes are s-planes. The p-plane used as bridge which provides carriers from charge reservoir to s-planes. The s-planes Cu atoms are known as Cu(2) and oxygen atom of this-plane is known as O(4). The oxygen atom linking the $Cu_{1-x}Tl_x Ba_2 O_{4-\delta}$ charge reservoir layer and p-plane is apical oxygen atom which is known as O(2) atom. This atom almost deals the charge transport mechanism from charge reservoir layer to p-plane. The O_3 atom or O_δ is the central oxygen atom of $Cu_{1-x}Tl_x Ba_2 O_{4-\delta}$ charge reservoir layer [48].

The major applications of superconductors in seven different regions are: electric powers, high engineering physics, transportations, medicines, industrial equipment, MRI

(magnetic resonance imaging technique), defense and space, electronics and communications [49].

1.6 Nanotechnology

The word “nano” comes from Greek word for “dwarf” which is equal to the one billionth of a meter or 10^{-9} m and one nanometer is nearly equal to 10 hydrogen and five silicon atoms, a human hair is 80,000 nm thick and a blood cell is approximately 7000 nm thick. Nanomaterials show the different physical properties as corresponding to bulk material [3, 50]. The following defining features of nanotechnology were struck out:

- Nanotechnology contains technology and research progress at the range of 1 nm to 100 nm.
- Nanotechnology generates and uses structures that have innovative properties due to their extremely small size.
- Nanotechnology builds on the aptitude to control or manipulate at the atomic scale.

Nanotechnology contains the major physical properties and phenomenon of nanomaterials and nanostructures which distinct it from bulk materials. Nanotechnology is probable to increase both quantitatively and qualitatively. Nanomaterials exhibit the high surface reactivity due to the large surface to volume ratio [51]. Nanotechnology generates new materials, devices with diverse applications [52] which have least efficient range in one dimension is on nanometer scale. The meaning of nanotechnology differs in every field but it is understood as “catchall”

description for anything very small [53]. Figure 1.10 describes the size comparison 1 m to 0.1 nm.

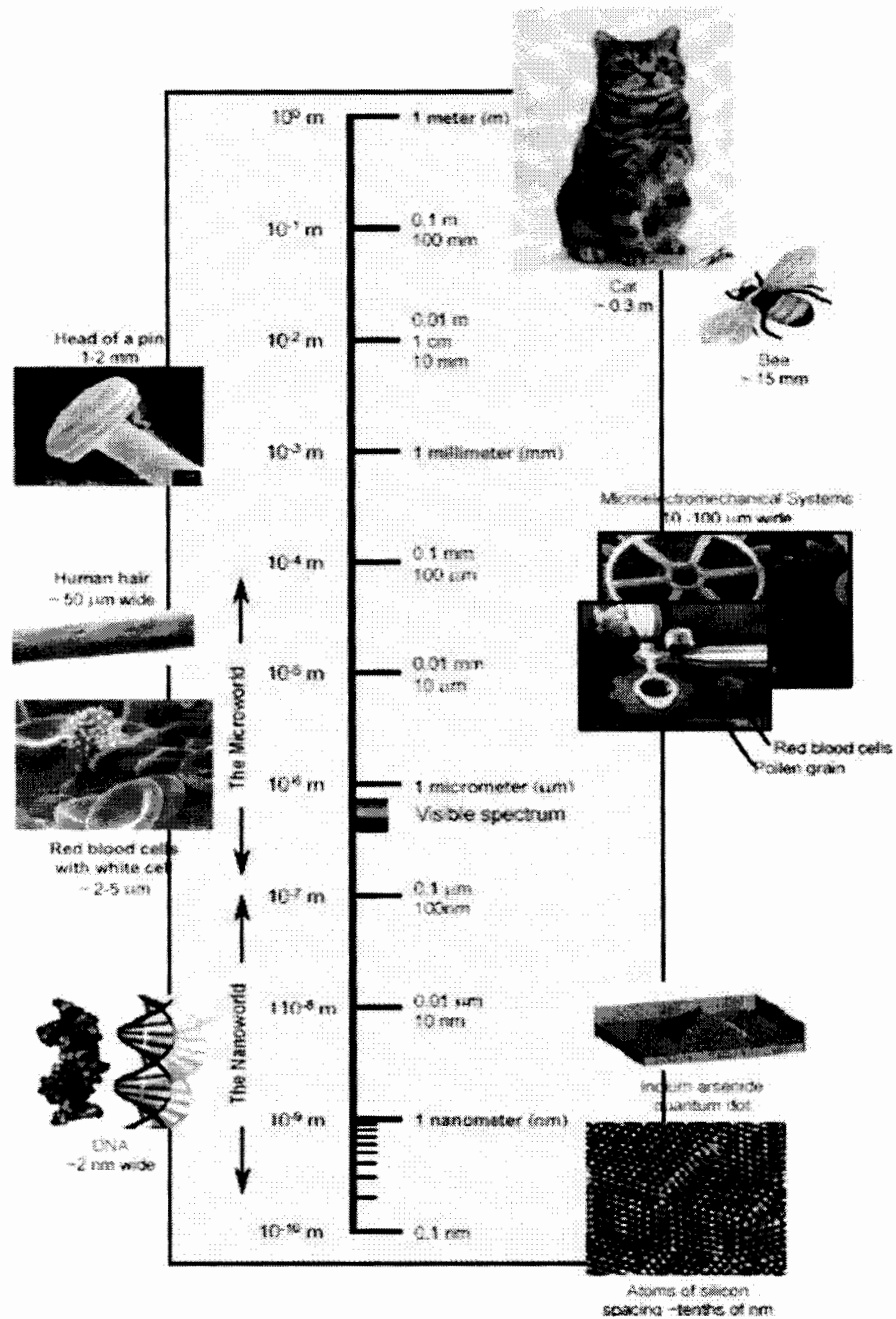


Fig. 1.10: Representation of size comparison (1 m to 0.1 nm) [54]

1.7 Nanoparticles

The particle which has a diameter ranges from 1 to 100 nm is called nanoparticle [55, 56]. They are found in nature and can also be prepared artificially. Figure 1.11 shows the SEM image of gold nanoparticles.

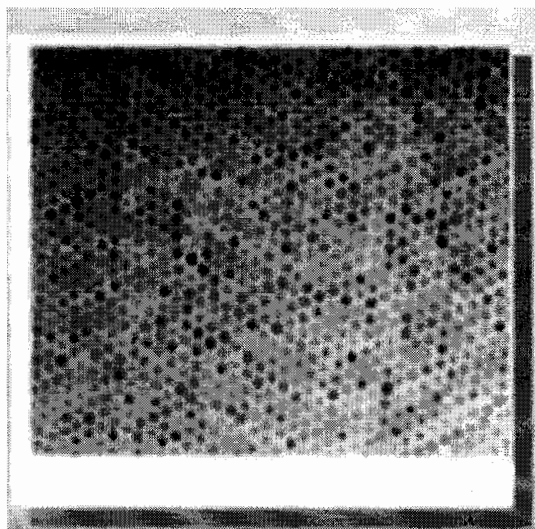


Fig. 1.11: SEM of gold nanoparticles [57].

In nanoparticles surface to volume ratio is very large due to their decreased diameters [58]. Nanoparticles exhibits different physical properties as compared to their bulk counter part due to quantum mechanical effect at nano-scale [59- 61]. Magnetic nanoparticles formed by reducing the grain size to the range of nanometer size have many practical applications. Magnetic nanoparticles are also very important in different areas e.g. biology, chemistry, medicine, geology and physics. One is the useful iron based magnetic nanoparticles are $ZnFe_2O_4$ nanoparticles which has the cubic normal spinal

structure. Ferrite basically obtained in the result of iron oxides combination with other oxides. Therefore they are related to the class of ferrimagnetic materials.

For technological point of view, it is important to synthesize nanoparticles having uniform particle size distribution, uniform shape, morphology, uniform chemical composition, and mono-dispersion i.e. no agglomeration [50]. So the nanotechnology uses in all branches of science such as in nanobots in practice of medicines [62], for DNA analysis [63], use the gold as catalysis [64], biological application [65], in engineering devices and molecular and nanotechnology electronics devices [66] and used to increase the magnetic data based storage of computer devices [67]. Figure 1.12 shows the applications of nanotechnology in different fields.

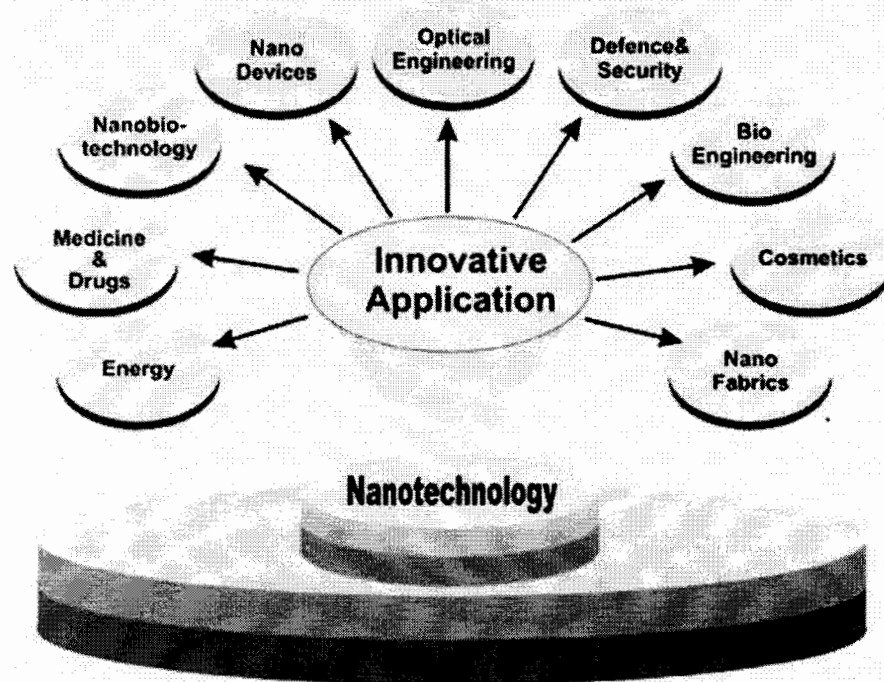


Fig. 1.12: Nanotechnology in different fields [66, 67].

1.8 Nanoparticles/superconductor composites

A group of materials formed from mixture of metals, ceramics or polymers in such a manner that unusual combination of properties is obtained [68]. The efficiency of high T_c superconductor in practical applications is often restricted due to the ductility and fragility [69], lower critical current density [70], and low anisotropy [71], substitution of nanoparticles can be used to reduce these problems in high T_c superconductors[72].

The ductility and fragility occurs in polycrystalline superconductor structure due to imperfections, grain boundaries, phase inhomogeneity and oxygen nonstoichiometric properties and improvement in all these properties is observed by the addition of 0.2 wt. % Al_2O_3 [73]. This can be improved by doping of nano- SnO_2 which increased the value fraction and phase without disturbing phases structure and improving the microhardness of specimen [74]. The addition of ZnO nanoparticles in $Cu_{0.5}Tl_{0.25}Pb_{0.25}-1223$ enhanced the critical temperature and volume fraction and resolves grain boundary resistance [75].

1.9 Motivation

High T_c CuTl-1223 superconductor is supposed to be very auspicious because of its higher critical temperature. The major issue of HTSCs is T_c and diamagnetism suppression, which is due to weak intergrain links, structural disorder, spin-spin interaction of the dopant etc.

This issue is addressed by many scientists by doping the superconductors with different elements and obtained the valuable results. Therefore many scientists doped the nanoparticles in superconductors due to their large surface to volume ratio with some surprising properties and got the favorable results. In the present research work, we have prepared the ferrite nanoparticles, separately synthesized the CuTl-1223 superconductor and superconductor composites which are prepared by doping of ferrite nanoparticles in CuTl-1223 superconductor. Chapter no. 02 contains the literature review to give information about the previous work. Chapter no. 03 deals with the synthesis methods (sol-gel method and solid state reaction method) and characterization techniques such as XRD, SEM, EDX, FTIR, resistivity and AC susceptibility used to prepare and study the nanoparticles/superconductor composites, respectively. Chapter no. 04 gives the information about new research results and their discussion.

Chapter # 2

Literature Review

L. Raffott *et al.* (1995) [76] studied the superconducting properties of $YBa_2(Cu_{1-x}Mg_x)_3O_{7-\delta}$ ($0 \leq x \leq 0.1$) and $La_{1.85}Sr_{0.15}(Cu_{1-x}Mg_x)O_4$ ($0 \leq x \leq 0.07$) superconductors. Their results supported the assumption that all nonmagnetic dopants have the same detrimental properties on superconductivity and are linked to the formation of a net magnetic moment in CuO_2 planes. It was observed that Mg substitution affects the temperature dependence of J_c and it exhibits no change in application of an external DC magnetic field.

G. Subramanyam *et al.* (1996) [77] prepared nearly single phase $TlBa_2Ca_1Cu_2O_8$ (2212) and $(Tl_{0.5}Pb_{0.5})Sr_{2-x}Ba_xCa_2Cu_3O_9$ (1223) superconductors. They found the growth of 2212 in two steps, heat treatment process and growth of single phase 1223 superconductor with finite Ba content of $x \geq 0.4$. The highest T_c (onset) was obtained 117 K at $x = 0.75$ with superconducting volume fraction over 50% and these results are significant for the processing of thin films of $(Tl_{0.5}Pb_{0.5})Sr_{2-x}Ba_xCa_2Cu_3O_9$ (1223) superconductors.

X. S. Wu *et al.* (1997) [78] concluded that structural variation due to Mg doping may vary the carrier's distribution which affects the superconductivity and physical properties by observing the $La_{1.85}Sr_{0.15}Cu_{1-y}Mg_yO_4$ superconductor with $0.0 \leq y \leq 0.30$.

R. Yanru *et al.* (1998) [79] analyzed the $TlBaCaCuO$ structure through XRD and electron micro probe. Superconducting transition gained at the range of 100-123 K. After observation it was concluded that the occurrence of high T_c may be depend upon the electron excitation at $\approx 0.1eV$ and phonon features at $\approx 850cm^{-1}$.

N. M. Hamdan *et al.* (1999) [80] observed the fluorine doping in $(Tl_{0.5}Pb_{0.5})Sr_{1.6}Ba_{0.4}Ca_2Cu_3O_y$. They examined the enhancements in superconductivity and its transport properties, enhancement of pinning strength, and increase in hysteresis loop, raised the critical temperature to 128 K and improved the critical current density to 300%.

F. J. Guaita *et al.* (1999) [81] were prepared Fe_2O_3 by ceramic method which is not suitable to exhibit as a $ZnFe_2O_4$ single phase at low temperature. This showed that ceramic is less reactive as compared to pechini method. EDX analysis shows the minor difference between nominal and sample composition, its means the synthesis avoided the decomposition of reaction. This technique shows the presence of Fe (III) but undetected in XRD. The results suggested the spinel $ZnFe_2O_4$ inversion, which established by magnetic measurements.

C. Liu *et al.* (2000) [82] synthesized the $CoFe_2O_4$ nanoparticles from a ferric salt with microemulsion method. The neutron diffraction confirmed the superparamagnetic nature of these nanoparticles and their superparamagnetic behavior, such as coercivity and blocking temperature correlates with particle size.

Z. Y. Jia *et al.* (2000) [83] studied that addition of ZrO_2 nanoparticles in $Bi_{1.8}Pb_{0.4}Sr_2Ca_{2.2}Cu_3O_{10+\delta}$ enhanced the critical current density due to trapping of nano-oxide particles with in grains of high temperature superconductors which appeared as secondary phase in the grains final compound

E. Kuzmann *et al.* (2001) [84] synthesized $(Bi_{0.93}Pb_{0.17})_2Sr_{1.9}Ca_{2.05}(Cu_{1.02}Fe_{0.01})_3O_y$ and $(Tl_{0.74}Bi_{0.25})(Ba_{0.2}Sr_{0.8})_2Ca_2(Cu_{0.99}Fe_{0.01})_3O_y$ superconductors by using Mossbauer spectroscopy and they found the decrease in the critical temperatures due to Fe led but the samples remained superconductors

F. Grasset *et al.* (2002) [85] were prepared the non-stoichiometric Zinc ferrite nanoparticle by using coprecipitation method and made it possible to prepare the design oxide nanoparticles.

S. Soltanian *et al.* (2003) [86] examined the flux pinning properties of MgB_2 superconductor by carbon nanoparticles addition. TEM results exhibited the carbon nanoparticle reacted with Mg to form polycrystalline Mg_2C_3 and MgB_2C_2 with nano-dimensions. TEM showed the enhancement of flux pinning in high field due to nanoparticles.

S. Y. Xie *et al.* (2004) [87] fabricated the copper nanoparticles, which has 10-15 nm mean diameter and collected via discharge of bulk copper rods in a cetyltrimethyl ammonium bromide acid solution. XRD results presented that prepared nanoparticles were CuO_2 and CuO and their size was calculated by Sherrer's formula.

Y. Jia *et al.* (2005) [88] prepared Co/Cu nanoparticles in hydrazine solution of copper chloride and cobalt chloride by sono-chemical method for the formation of fcc cobalt, at temperature 60°C.

B. P. W. Rao and O. F. Caltun (2006) [89] described the synthesis of some ferrite nano particles by using the ceramic method and ball milling method. The size and structure of the nanoparticles obtained through XRD technique which lies between 2-16 nm and consist on single phase cubic spinal structure with smaller magnetization.

C. Yao *et al.* (2007) [90] synthesized the $ZnFe_2O_4$ nanocrystals by thermal deposition method with average size 9.8 nm. They obtained ferromagnetic structure of the particles from magnetization data and the saturation magnetization is obtained $44.9 \text{ emu}\hat{a}g^{-1}$ at room temperature.

Y. Xu *et al.* (2008) [91] discussed the collective ZrO_2 and ZnO nanoparticles behavior in Gd-123 bulk superconductor and obtained J_c enhancement but suppression in T_c due to Zn ion substitution in Cu site.

S. G. Elsharkawy and R. Awad (2009) [92] studied the lattice parameter variation and the volume thermal expansion for $(MgO)_x Cu_{0.25} Tl_{0.75} Ba_2 Cu_4 O_{12-\delta}$. They observed the improvement in phase structure, grains connectivity and thermal coefficient reduction. Thermal volume expansion divided in two parts. First one temperature decreases, α decreases rapidly and in second α decreases slowly when temperature decreases.

N. H. Mohammad *et al.* (2010) [93] studied the $Cu_{0.5}Tl_{0.5}-1223$ phase formation, mechanical and electrical properties, and microstructure by the addition of SnO_2 and In_2O_3 nanoparticles. The microhardness of $Cu_{0.5}Tl_{0.5}-1223$ increased by doping SnO_2 nanoparticles ($x= 1.0$ wt. %) but decreased after $x= 0.1$ wt. % of In_2O_3 addition. They also showed that some mechanical parameters depend upon the SnO_2 and In_2O_3 nanoparticles. They finally obtained that nano- SnO_2 increases the mechanical parameters and In_2O_3 improved the ductility and reduced the brittleness of the $Cu_{0.5}Tl_{0.5}-1223$.

M. Farbod and M. R. Batvandi (2011) [94] described the Ag nanoparticles effect on critical current. They concluded the enhancement of J_c after doping of different size nanoparticles in superconductor bulk sample.

N. A. Khan *et al.* (2012) [95] discussed the $CuTl-1223$ properties with doping of CuO_2 nanoparticles, which enhanced critical current (T_c), current density (J_c) with increasing concentration of nanoparticles.

Chapter # 3

Synthesis and Experimental Techniques

3.1 Synthesis of superconductors

As the time passed, new synthesis methods have been developed for the high temperature superconductors [96, 97]. The common well known method is solid state reaction method or ceramic method which is used for oxide materials synthesis [98]. By using this method best results can be achieve from the characterization of high temperature superconductors. It is necessary to control some issues about cation configuration, oxygen stoichiometry, cation oxidation state and carrier concentration. If all the components are solids, the method is called ceramic method and their synthesis method depends upon the material nature, homogenous powder mixing, heating rate and as well as reaction temperature and duration. The preliminary materials which are metal oxide, carbonates nitrate or other salts after homogeneous mixing prepared in sealed evacuated capsule and heating at given temperature.

3.2 Synthesis of nanoparticles

Synthesis of nanoparticles has two main approaches such as top down approach and bottom up approach as shown in Fig. 3.1.

3.2.1 Top down approach

Top down approach is a method in which a bulk piece of material sculpted into small nano-sized pieces. It has further four techniques; lithography, high energy ball milling, gas condensation technique and sever plastic deformation.

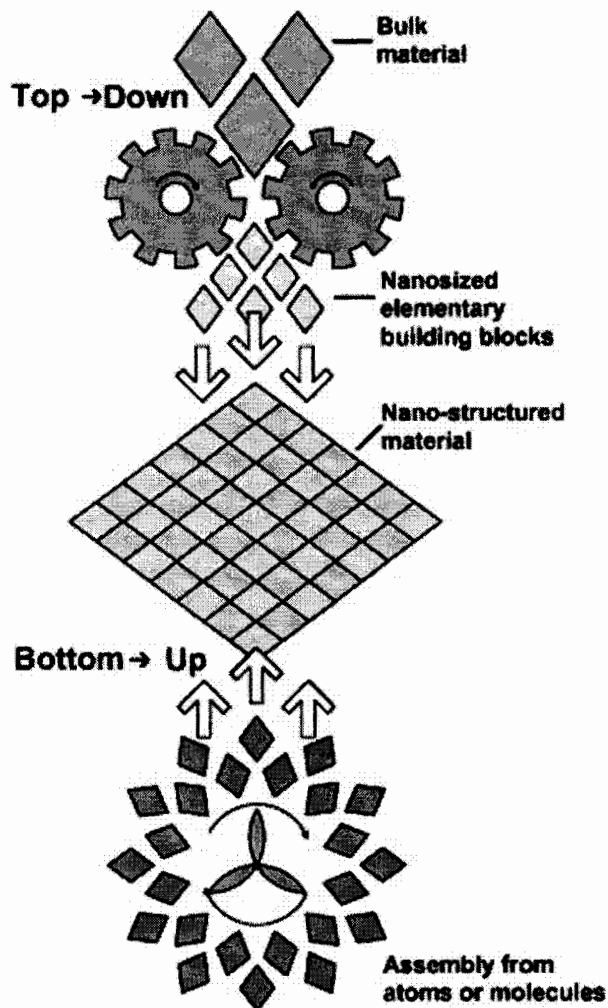


Fig. 3.1: Top down and bottom up approach to synthesize nanoparticles [53].

3.2.2 Bottom up approach

Nanostructure and nanomaterial built from the basic building blocks such as atom by atom, molecule by molecule and cluster by cluster. These building blocks are automatically self-assembled and can be arranged into designed nanostructured morphology. It has further five techniques; physical vapor deposition, chemical vapor deposition, sol-gel method, self-assembly and soft lithography [53]. Among all these synthesis methods, sol-gel method has advantages over other methods because it gives narrow particle size distribution and is low cost. It is a useful technique for the fabrication of materials due to its less surface defect and highly pure properties [50].

3.3 Synthesis of nanoparticles/superconductor composites

$Cu_{1-x}Tl_xBa_2Ca_2Cu_3O_{10-\delta}$ bulk superconducting sample with doping of $(ZnFe_2O_4)_y$ ($y = 0, 0.05, 0.1, 0.15, 0.2, 0.25, 0.5, 1$ and 2%) oxide nanoparticles. The method which is used to prepare these samples is known as the solid state reaction method. The sample preparation process was completed in three stages.

At first stage, $Cu_{1-x}Tl_xBa_2Ca_2Cu_3O_{10-\delta}$ superconducting material was prepared by using precursors of $Cu(CN)$, $Ba(NO_3)_2$, and $Ca(NO_3)_2$ preliminary compounds. These compounds were mixed in appropriate ratios (4.845 g, 7.34 g and 2.811 g respectively) in quartz mortar and pestle. Completely fine ground material was fired at 860°C for 24 h in quartz boat in air till cool down the furnace to room temperature and added the 0.272 g

Tl₂O₃ in this material to attain the host superconductor matrix as shown in schematic diagram Fig. 3.2.

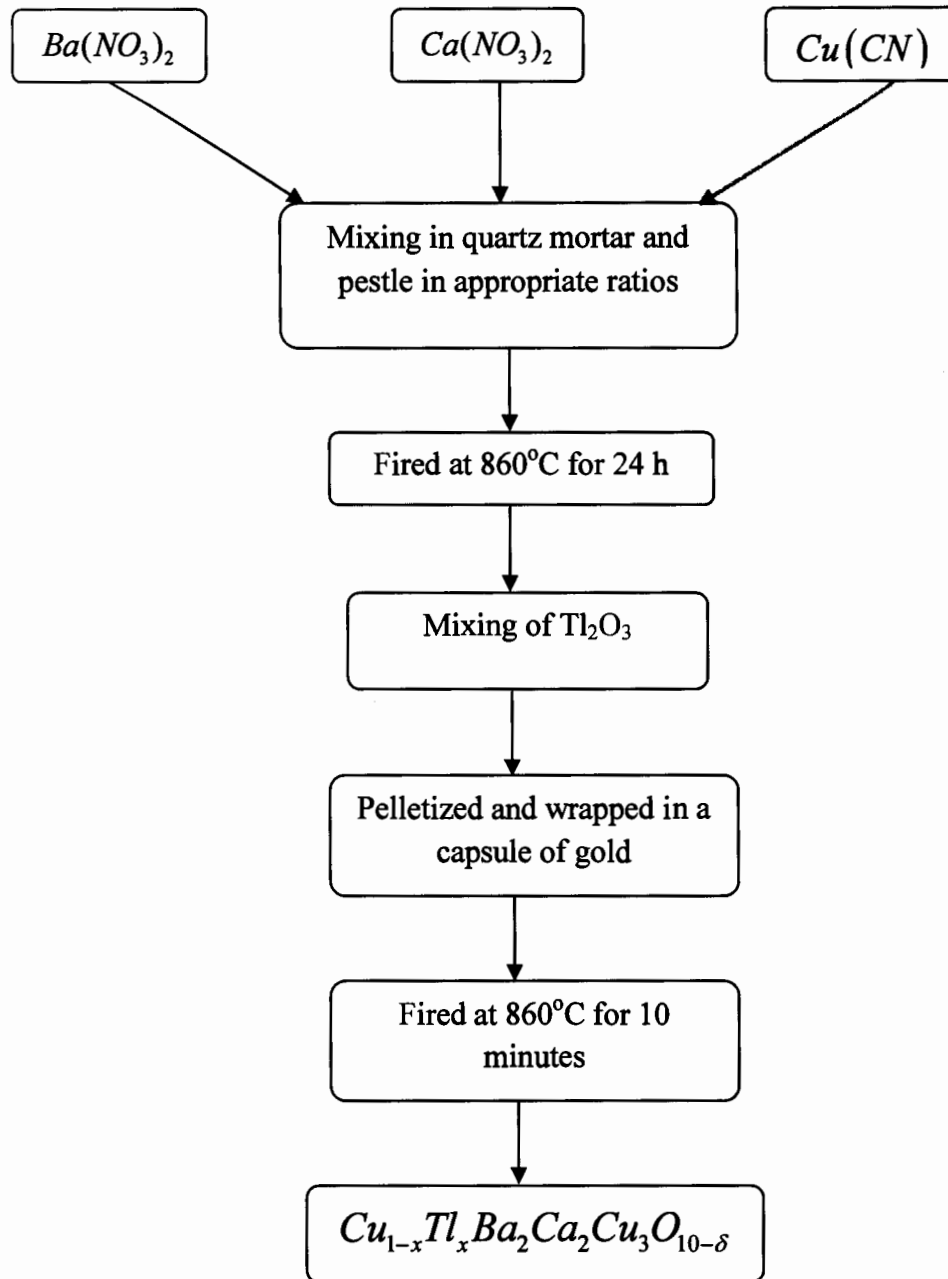


Fig. 3.2: Schematic diagram to synthesize $Cu_{0.5}Tl_{0.5}Ba_2Ca_2Cu_3O_{10-\delta}$ superconductor.

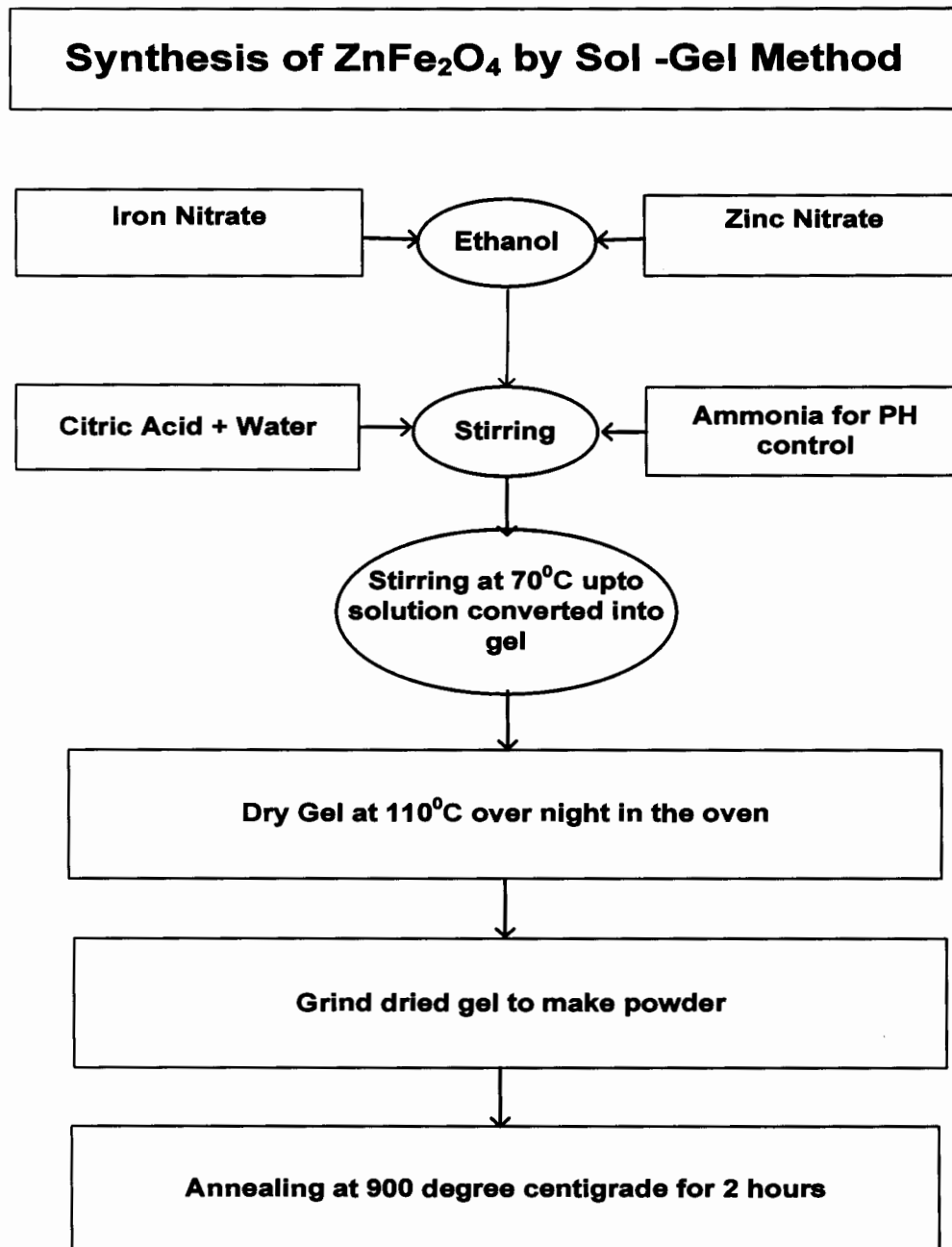


Fig. 3.3: Schematic diagram to synthesize $ZnFe_2O_4$ nanoparticles by sol-gel method.

At the second stage, $ZnFe_2O_4$ nanoparticles were prepared by sol-gel method as shown in Fig. 3.3. After necessary calculations for all the chemicals we weighted them and then made the solution of the zinc nitrate and iron nitrate in the ethanol by stirring. Similarly, solution of the citric acid and water (1: 4) was prepared after stirring. Then we have added drop by drop the solution in to the solution of zinc nitrate and iron nitrate. At the end we adjusted the pH of the solution to 5 by adding ammonia into the solution. After this we switched on the hot plate and adjusted a thermometer to note the temperature. Temperature was adjusted in the range of 70-75⁰C. When the gel was formed the beaker was placed in the oven at temperature 110⁰C to dry the gel. At the end we grinded the dried gel and made powder of it.

TH 9359
A calculated amount of ferrite ($ZnFe_2O_4$) nanoparticles in different weight percent were added in as prepared superconducting material and then ground for an hour. Thoroughly mixed material was fired at 860⁰C for 24 h into a preheated furnace and furnace cooled to room temperature.

As shown in the Fig. 3.4 at the third stage, initially prepared material having both superconducting material and nanoparticles were then ground for about an hour. After grinding, Tl_2O_3 was added in an appropriate wt. % e.g in 1% 0.3929 g. Thallium mixed composite were palletized under 5 ton/cm² pressure by using hydraulic press from carver and pallet were enclosed in a gold capsule. Gold capsule containing pallets was annealed about 10 minutes at 860⁰C followed by quenching to room temperature and finally we got desired CuTl-based nanoparticles/superconducting composites.

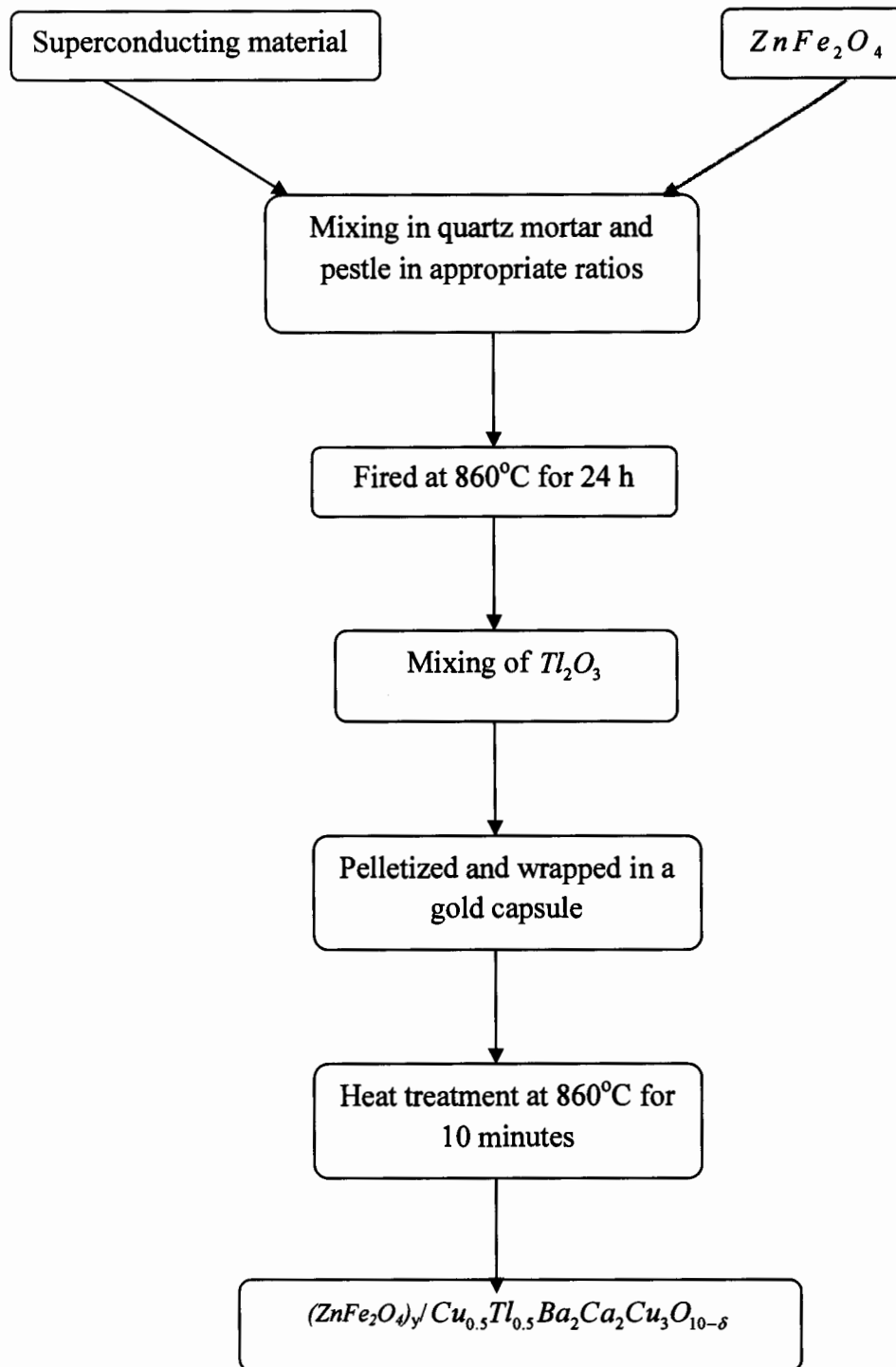


Fig. 3.4: Schematic diagram to synthesize $(ZnFe_2O_4)_y / (Cu_{0.5}Tl_{0.5})Ba_2Ca_2Cu_3O_{10-d}$ nanoparticles/superconductor composites.

3.4 Experimental techniques

The samples were characterized by using different experimental techniques as described in sections 3.4.1 – 3.4.6.

3.4.1 X-ray diffraction (XRD)

X-ray diffraction (XRD) is a tool which is used to investigate the fine matter structure. In 1912, Von Laue's discovered that crystal diffracts X-ray which reveals the crystal structure. At earlier times, it was used only for the study of crystal structure but with the development of technology, now it is possible to get the information about crystal geometry e.g. lattice constant, chemical analysis, measurement of particle size and orientation of crystal planes [99]. A collimated beam of X-ray with wavelength of 0.7 to 2 Å is incident to the specimen.

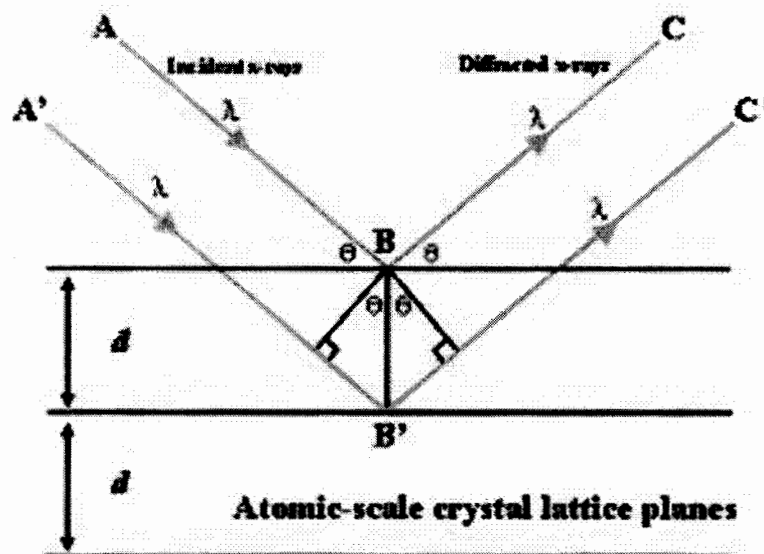


Fig. 3.5: Diffraction of X-rays from crystal planes [2].

Figure 3.5 shows the diffraction of X-rays from crystalline planes of specimen. According to the Bragg's law,

$$2d \sin\theta = n\lambda \quad (3.1)$$

Where n has integral values, d = spacing between atomic planes and λ = wavelength of X-ray. The schematic diagram of an X-ray diffraction is shown in Fig. 3.6.

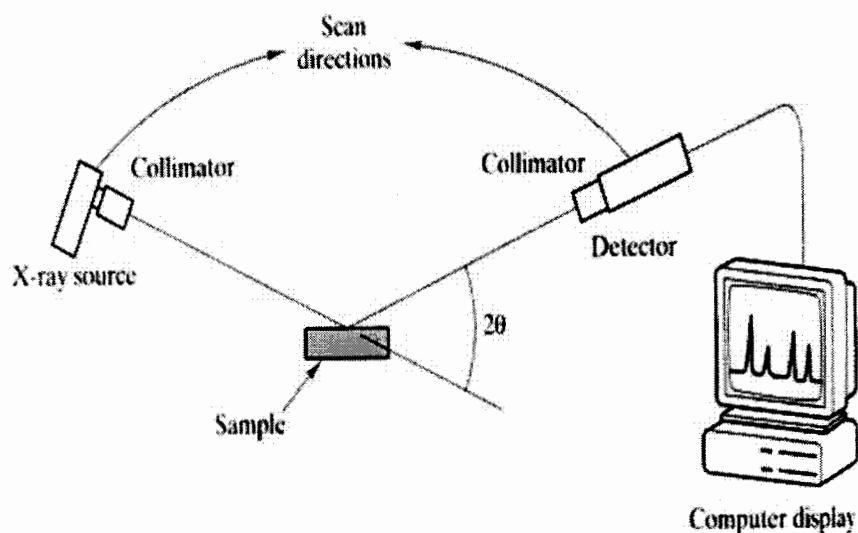


Fig. 3.6: X-ray diffraction scheme [47].

X-rays produced by ionization of electrons from the K-shell are used for the diffraction analysis due to its shorter wavelength as compared to those X-rays from L-M shell. The most common target materials are copper (Cu) and molybdenum (Mo) used to produce X-rays with wavelength 1.54 to 0.8 Å [100, 101]. The crystalline size “D” can be calculated from Scherrer's formula

$$D = \frac{0.9\lambda}{\beta \cos \theta} \quad (3.2)$$

where D = particle size, λ = wavelength of X-ray, θ = Bragg's angle and β = full width at half maximum (FWHM) [102].

3.4.2 Scanning electron microscopy (SEM)

The SEM is the most extensively useful technique of all electron beam mechanisms. The SEM importance has been raised due to its several imaging modes, excellent images resolution, generated micrographs can be easily interpreted, no need of sample preparation, user-friendly technique, and now its resolution can approach to 0.5 nm and it can handle the specimens size as large as production size silicon wafers. The SEM is a mapping technique, rather than an imaging technique.

A beam of electron used as a probe and is scanned across the sample surface. Signals (Secondary electrons) from the sample are identified, amplified and then used to modulate the brightness of second beam of electron of a cathode ray tube. The two beams synchronously scanned. An electron beam produced by electron gun may either thermionic or field emission, is focused by condenser lenses and the objective lens determines the final spot size of electron beam scanned on the sample surface in a raster pattern in synchronization with CRT beam. Interaction of electron beam with sample gives rise to the various signals [103]. Figure 3.7 shows the schematic diagram of SEM.

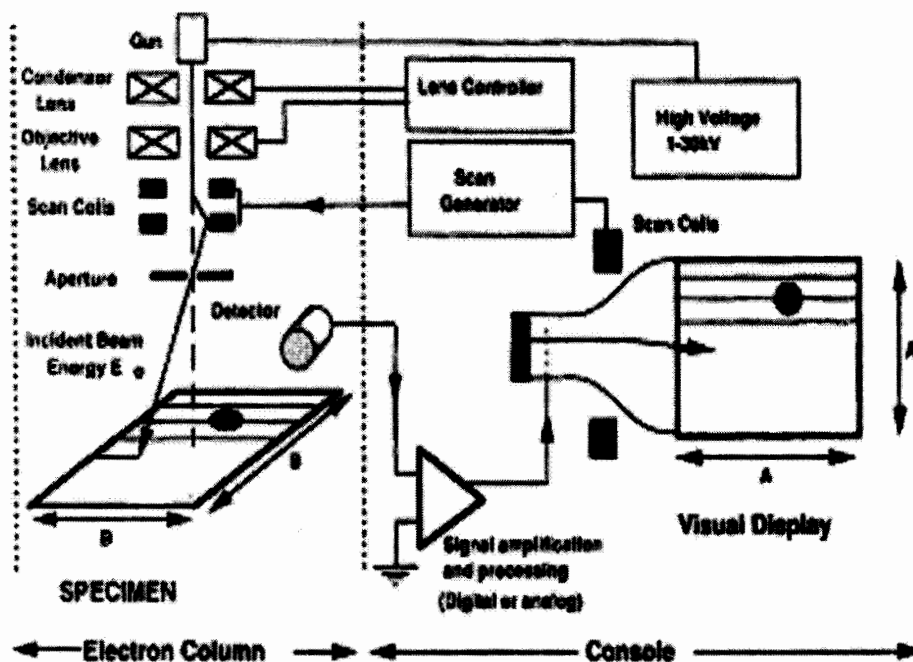


Fig. 3.7: SEM schematic diagram [103].

3.4.3 Energy dispersive X-ray analysis (EDX)

The analyzing technique which is used to identify the specimen elemental composition is known as EDX (energy dispersive X-ray analysis). The EDX technique acts as an integrated feature of a scanning electron microscope (SEM). To estimate the emission of characteristic X-rays from specimen, a high energy beam of electron or X-rays, is focused into the specimen. At rest, an atom within the sample contains unexcited electrons in discrete energy levels bound to the nucleus. The incident beam may excite an electron in an inner shell, ejecting it from the shell while generating hole. An electron from an outer higher-energy shell then fills the hole, and the difference in energy between the higher energy shell and the lower energy shell may be released in the form of an X-ray.

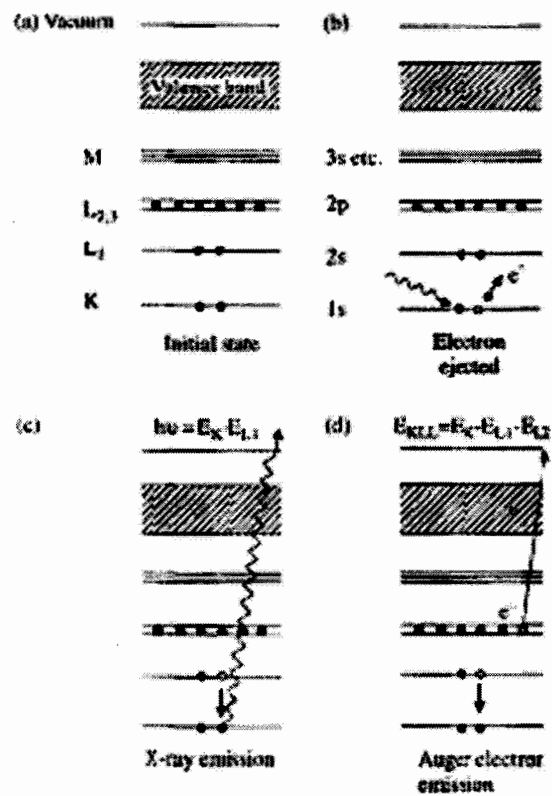
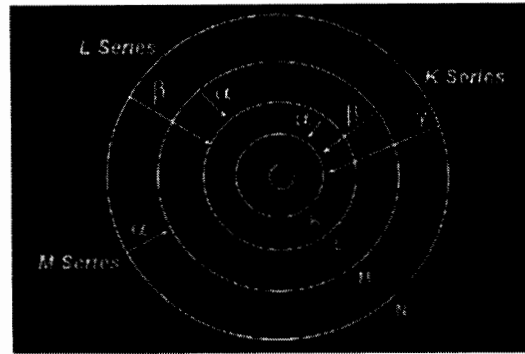


Fig. 3.8: EDX spectrum, transfer of electron from high energy shell to low energy shell [48].

An EDX spectrum normally exhibits the relation of peaks and energy levels and explains the type of X-rays. For example if the electron transition is occurred from L-shell to K-shell than its peak identified as K-Alpha peak. Similarly if the transition of an electron is occurred between M-shell to K-shell than its peak identified as K-Beta peak. [48].

3.4.4 Fourier transforms infrared (FTIR) spectroscopy

A technique which is most suitable to detect molecular vibration is known as Fourier transforms infrared (FTIR) spectroscopy [50]. Its basic principle depends upon the Michelson interferometer as shown in Fig. 3.9.

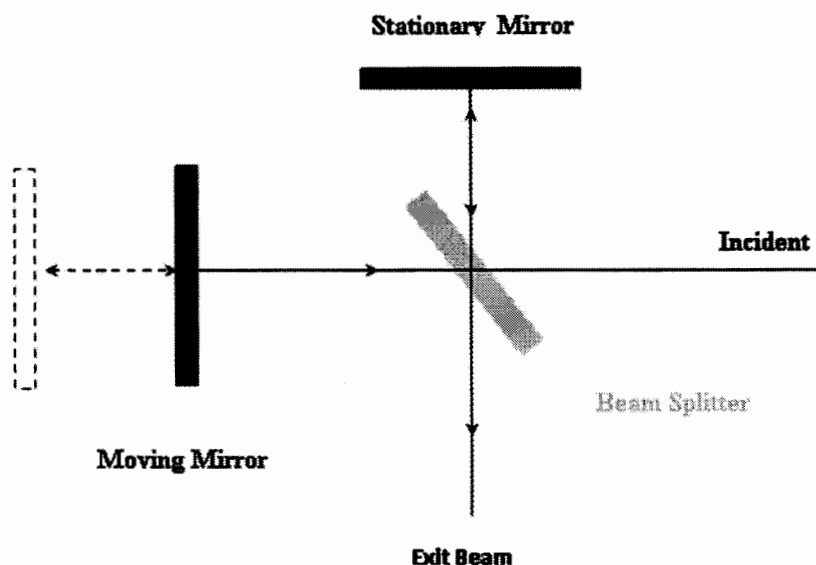


Fig. 3.9: Michelson interferometer schematically [47]

Commonly the fundamental lattice vibrations are not equal to the absorption band. The radiations absorbed into sample due to same frequency and associated energy converted into these types of motion. FTIR spectroscopy of the samples was done by using KBr pellet technique. In this technique, sample was prepared in a thin pallet shape by mixing small quantity of sample material which sufficient amount of KBr. Firstly background spectrum was collected with KBr pellet and then sample spectrum was observed. The spectrometer subtracted the background spectrum and exhibits the sample spectrum. It appeared after taken the number of scans for background and 10 to 50

number of scan of the sample. In high temperature superconductor for interpretation of results, lattice dynamical calculation was used and in superconductor sample it is very helpful to assign the vibrations mode to particular atom.

3.4.5 Resistivity measurement setup

All the superconducting properties are based on the resistivity phenomena. The causes of the resistivity of metals are due to lattice imperfections, lattice vibrations and electron-electron scattering [104]. A schematic diagram of the resistivity setup is shown in Fig. 3.10.

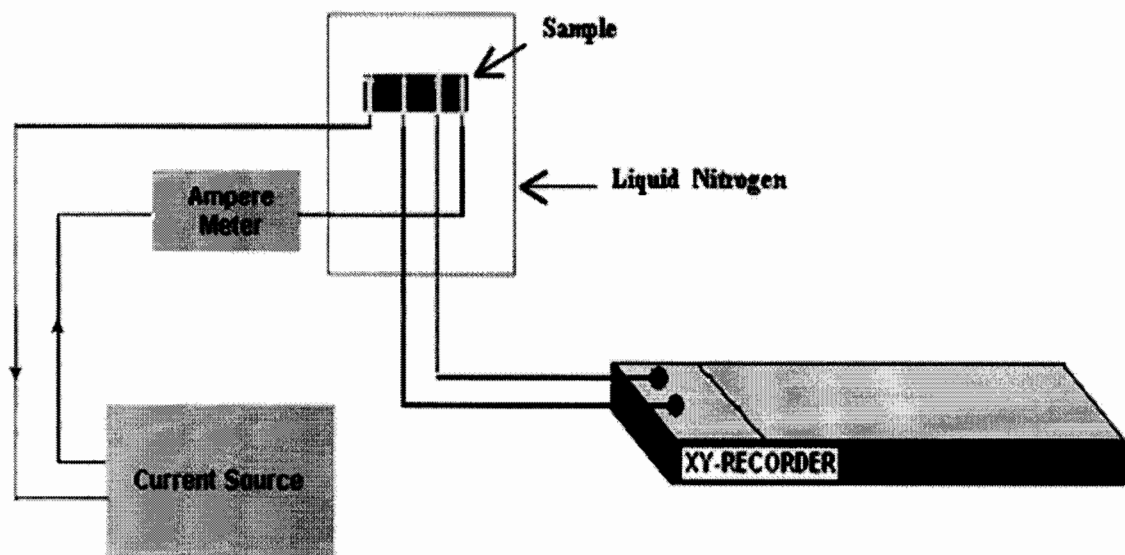


Fig. 3.10: Resistivity setup [47].

The transition of resistivity exhibits the doping carriers role in materials, either they increase or decrease the critical temperature T_c . The four probe technique is used for resistivity measurements. In this technique four leads are adjusted on the sample surface

and silver paint (low contact resistance) is used to attach them with sample. The outer leads were used to supply a constant current and voltage drop was measured from middle leads. A homemade cryostat was used for cooling the sample down to 77 K [46].

The resistivity of the material can be calculated by using the following formula,

$$\rho = \frac{V(T)A}{IL} \quad (3.3)$$

where $V(T)$ = voltage drop across the sample, A = cross-sectional area of the sample,

L = length of the sample and I = current through the sample.

3.4.6 AC susceptibility measurement setup

The magnetic behaviour of the specimen under applied magnetic field is known as its susceptibility. The notation χ is usually used to denote the susceptibility. It has two types, DC susceptibility and AC susceptibility.

If the DC magnetic field is applied without change w.r.t time then susceptibility is called DC susceptibility (χ_{dc}) and given by Eq. 3.4

$$\chi_{dc} = \frac{M}{H_{dc}} \quad (3.4)$$

where M is the magnetization of the material and H is the applied field.

In AC susceptibility, AC magnetic field is applied on the sample and magnetization changes are measured. It has the following expression [105].

$$\chi_{ac} = \frac{dM}{dH_{ac}} \quad (3.5)$$

AC susceptibility has two components, one is the real part or in-phase of $\chi_{ac} = \chi'$ and the other is imaginary (out of phase) part of $\chi_{ac} = \chi''$. The real part of χ is in phase with H, while imaginary part is out of phase with H by 90° . This real part is often called diamagnetic susceptibility and is equal to the derivative dM/dH ; whereas the imaginary part is related to the energy losses due to magnetic field cycling within superconducting sample. Below the time domain diagram of χ' and χ'' as shown in Fig. 3.11.

$$\chi = \chi' + i\chi'' \quad (3.6)$$

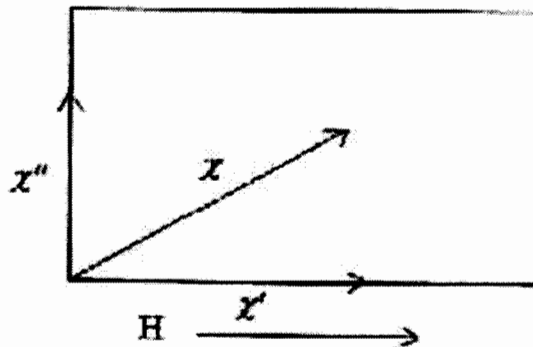


Fig. 3.11: AC susceptibility phase diagram where H is applied magnetic field [48].

The real part of AC susceptibility explains the relation among the magnetic spins clusters and defines the magnetic response of the system. It provides the information about dislocations, transition temperature or transition width present in different magnetic materials. The imaginary part is out of phase reflects the incapability of system to follow the vicissitudes of system in applied magnetic field totally in coherence or in phase with it and also shows the energy dissipation in the magnetic system. The schematic block diagram of the system is shown in Fig. 3.12. The primary and secondary coils were

wound by using a copper wire. The sample was placed in lower portion of secondary coil and cooled down to 77 K in a liquid nitrogen dewar.

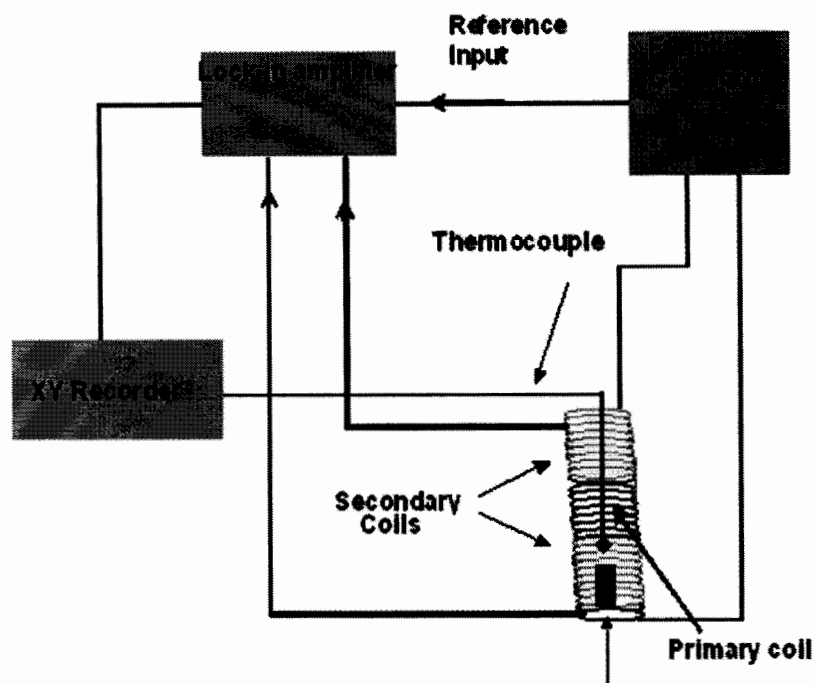


Fig.3.12: AC susceptibility setup [47].

A one volt signal at 270 Hz was applied from a function generator “Model HP 3314A” and amplified using a lock in amplifier “Model SR 530”. The decrease in critical temperature was also observed when frequency value higher than 270 Hz. A thermocouple fitted in the intermediate vicinity of sample was used for temperature measurements. The susceptibility graph was plotted on XY-recorder.

Chapter # 4

Results and Discussion

The most remarkable and amiable family of high temperature superconductors (HTSCs) is $Cu_{0.5}Tl_{0.5}Ba_2Ca_{n-1}Cu_nO_{2n+4-\delta}$ [$Cu-12(n-1)n$]; $n = 2, 3, 4, \dots$, because of its least anisotropy ($\gamma = 5$) and along c-axis exhibits the long coherence length [106]. It consists of a charge reservoir layer $Cu_{0.5}Tl_{0.5}Ba_2O_{4-\delta}$ and three CuO_2 conducting planes. The addition or subtraction of oxygen in charge reservoir layer could be controlled by the concentration of carriers in CuO_2 planes [107]. The superconductivity is affected by doping of impurity in HTSCs due to their different electronic configuration and interaction with free carriers which can increase or decrease the superconducting properties such as; high transition temperature (T_c), high aptitude to transmit electrical current, and low anisotropy parameter [108, 109]. But in some cases small doping can demolish the large part of superconductivity [110]. To improve the superconducting properties the researchers have substituted the nanoparticles in superconductors and have attained different results. Nanoparticles addition can affect the flux pinning in the superconductor. The MgB_2 superconductor showed the improvement in flux pinning due to the doping of SiC nanoparticles. The depression of T_c in MgB_2 bulk superconductor was observed due to the carbon nanoparticles doping [111].

Properties of the (Bi, Pb) -2223 superconductor can be changed by the addition of Al_2O_3 nanoparticle. The decrease in critical current density (J_c) and transition temperature

(T_c) was observed due to the addition of maximum wt. % of Al_2O_3 nanoparticles in (Bi, Pb) -2223 superconductors [112]. The variation in superconducting properties of MgB_2 superconductor was observed due to the doping of high reactive Fe nanoparticles which decreases the T_c and J_c [113]. The doping of MgO nanoparticles improves the J_c and T_c of Bi -2212/ Ag superconductor tapes [86]. The increase in normal core pinning of Gd -123 was studied with the substitution of ZrO_2 nanoparticles [114] and ZnO addition can also increase the J_c of Gd -123 bulk superconductors [115]. The small wt. % of MgO nano-oxides enhanced the microhardness, grain connectivity and critical current of $Cu_{0.5}Tl_{0.75}$ -1234 superconductor but decrease the above properties by addition in large number [89]. The SnO_2 nanoparticles enhanced the microhardness of $Cu_{0.5}Tl_{0.5}$ -1223 superconductor and improve the grains porosity [116]. The antiferromagnetic reduction investigated by doping of Zn in $CuTl$ -1223 superconductor which increased the carrier's density in conducting planes [90]. The microhardness of $Cu_{0.5}Tl_{0.5}$ -1223 superconductor increases as the SnO_2 nanoparticles doping gradually increases likely similar results gained at 0.1% addition of In_2O_3 nanoparticles and after this range it decreases [73]. The ZnO nanoparticles improved the phase and volume fraction of $Cu_{0.5}Tl_{0.25}Pb_{0.25}$ -1223 superconductor at low concentrations [72]. The critical current density and grains connectivity of $YBa_2Cu_3O_{7-\delta}$ bulk superconductor enhanced due the addition of Ag nanoparticles in [15]. The addition of NiO nanoparticles in Bi - Sr - Ca - Cu - O superconductor decreased the T_c and J_c due to the increase of disorientation of grains and agglomeration of nanoparticles in grain boundaries [117].

In this research work, we have studied the superconducting properties of $Cu_{0.5}Tl_{0.5}Ba_2Ca_2Cu_3O_{10-\delta}$ ($CuTl-1223$) superconductor substituted by $ZnFe_2O_4$ nanoparticles. The solid state reaction method is used to prepare these composites at 860°C in different nanoparticle compositions such as 0, 0.05, 0.1, 0.15, 0.2, 0.25, 0.5, 1 and 2%. These superconductor samples have been characterized by the following techniques as explained in chapter 3.

4.1 X-ray Diffraction (XRD)

The Bruker D8 advance X-ray Diffraction instrument is used to analyze the crystal structure of nanoparticles/superconductor composites. In our research work the best fitted data is obtained by computer software “Check cell”, which provides the peaks data, identifies the crystal structure and also provide lattice parameters. The X-ray Diffraction (XRD) scan of $ZnFe_2O_4$ nanoparticles is presented in the Fig. 4.1. By using Debye-Scherrer’s formula, the average calculated size of $ZnFe_2O_4$ nanoparticles is 28 nm.

$$D = \frac{0.9\lambda}{\beta \cos \theta} \quad (4.1)$$

where D = particle size, λ = wavelength of X-ray, θ = Bragg’s angle and β = full width at half maximum (FWHM). All the indexed peaks correspond to spinel Zn- ferrite and there is no evidence of the impurities. The $ZnFe_2O_4$ nanoparticles exhibit the high crystallinity which is evident by the sharpness of the peaks.

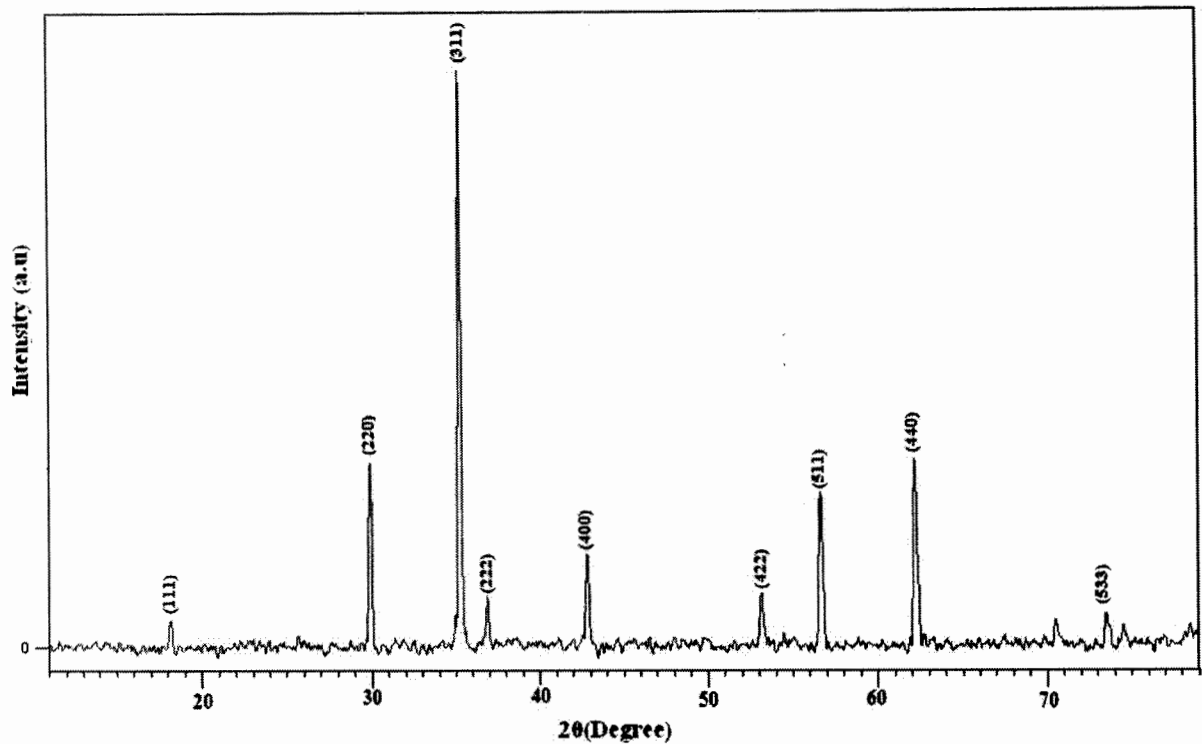


Fig. 4.1: XRD pattern of $ZnFe_2O_4$ nanoparticles.

The XRD scans of few $(ZnFe_2O_4)_y / (Cu_{0.5}Tl_{0.5})Ba_2Ca_2Cu_3O_{10-\delta}$ composites are shown in the Fig. 4.2. The major diffraction peaks are well fitted to tetragonal structure following P4/mmm space group. The un-doped CuTl-1223 superconductor sample has phase lattice parameters $c = 14.21 \text{ \AA}$ and $a = 4.19 \text{ \AA}$. The substitution of $ZnFe_2O_4$ nanoparticles in CuTl-1223 superconductor does not alter its cell parameters and structural symmetry. The c-axis length of $ZnFe_2O_4$ nanoparticles doped samples are $c = 14.22 \text{ \AA}$, 14.20 \AA and 14.19 \AA with 0.1, 0.5 and 2% wt. %, respectively. The slight fluctuation in c-axis length could be due to the variation of oxygen (O_δ) at the grain boundaries. The major obtained phase peaks are CuTl-1223 which is our required phase but some other impurity phases are also present.

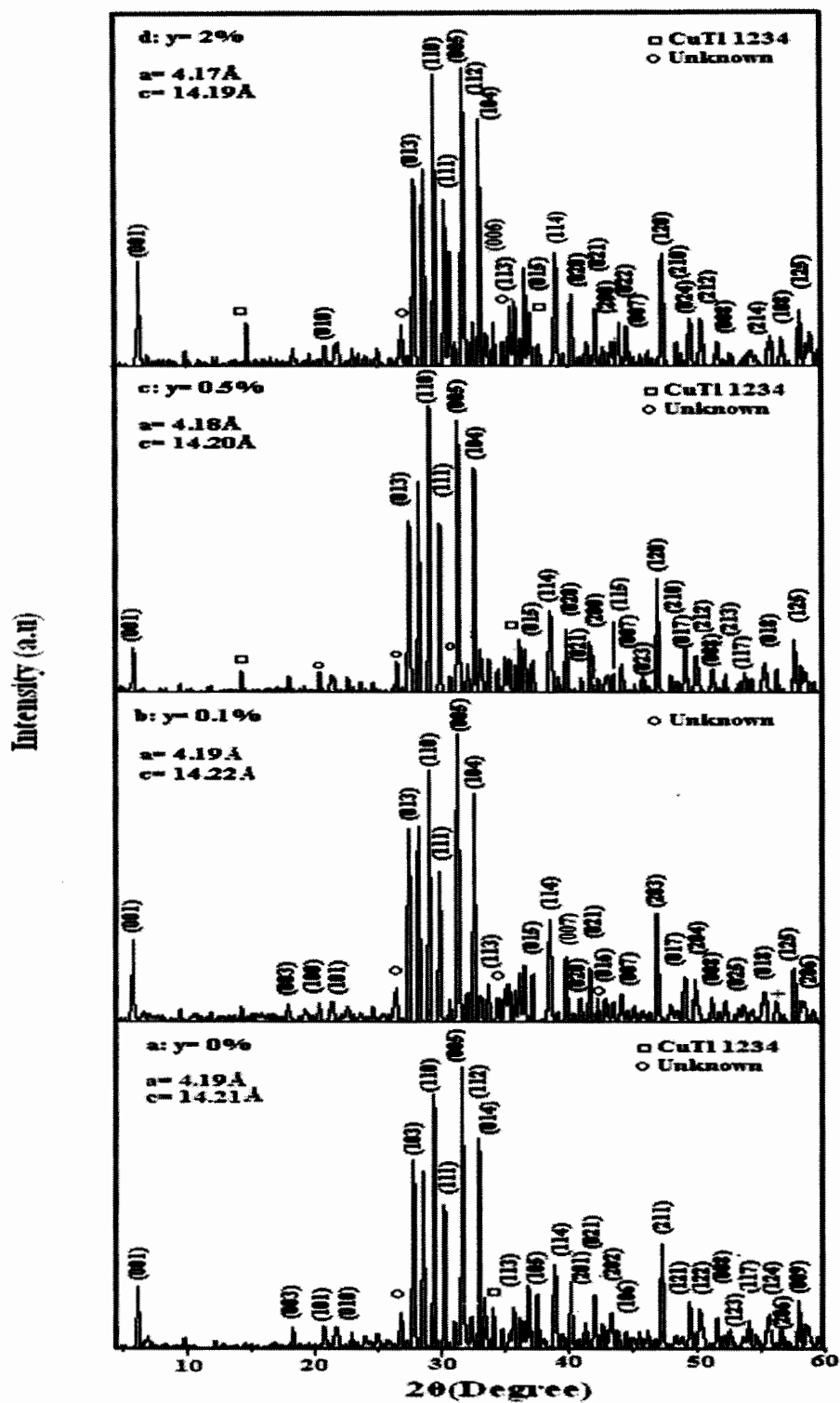


Fig. 4.2: XRD patterns of $(\text{ZnFe}_2\text{O}_4)_y/(\text{Cu}_{0.5}\text{Ti}_{0.5})\text{Ba}_2\text{Ca}_2\text{Cu}_3\text{O}_{10-\delta}$ composites a: $y = 0\%$, b: $y = 0.1\%$, c: $y = 0.5\%$ and d: $y = 2\%$.

4.2 Scanning electron microscopy (SEM)

The SEM images of $(ZnFe_2O_4)_y / (Cu_{0.5}Tl_{0.5})Ba_2Ca_2Cu_3O_{10-\delta}$ ($y = 0$ and 1%) superconductor composites are shown in Fig. 4.3(a, b).

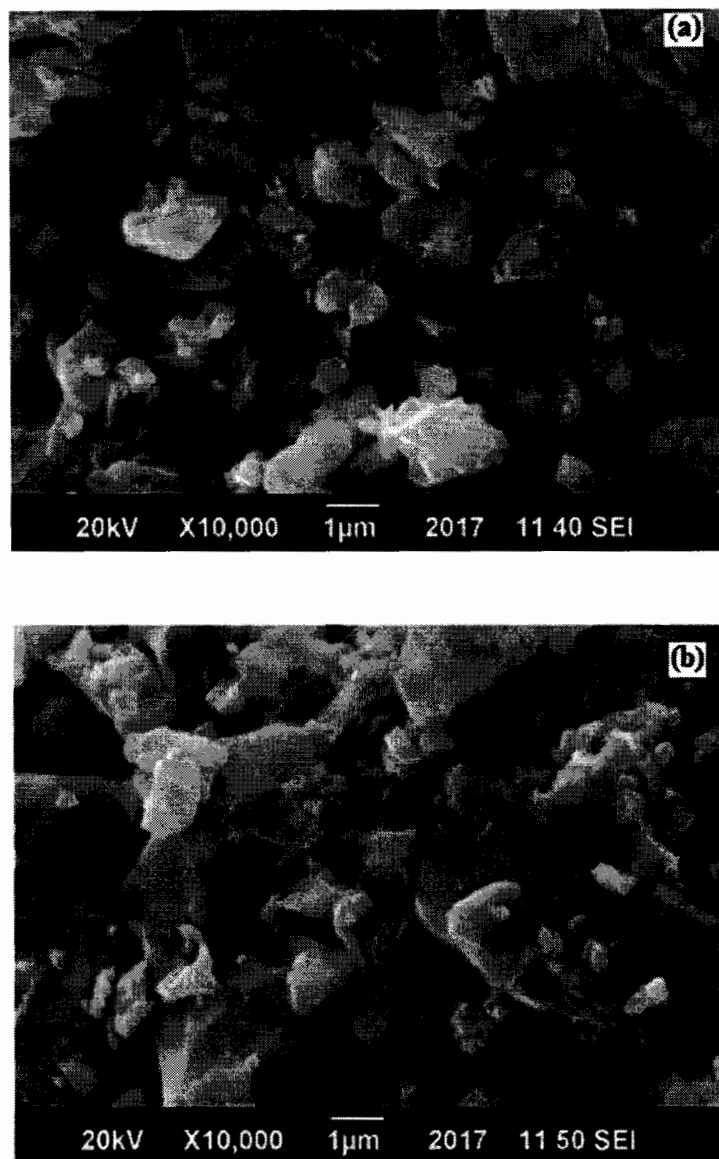


Fig. 4.3: (a) SEM image of $Cu_{0.5}Tl_{0.5}Ba_2Ca_2Cu_3O_{10-\delta}$ superconductor, (b) SEM image of $(ZnFe_2O_4)_y / (Cu_{0.5}Tl_{0.5})Ba_2Ca_2Cu_3O_{10-\delta}$ superconductor composite with $y = 1\%$.

The SEM images signify the granular and porous structures of host CuTl-1223 superconductor matrix. Figure 4.3 (a) clearly displays the weak grain connectivity, high porosity and disorientation of grains in un-doped CuTl-1223 superconducting sample due to inhomogeneous precursor mixing. Figure 4.3 (b) shows the minor difference in before and after doping sample due to the presence of *very small percentage* of $ZnFe_2O_4$ nanoparticles. This means that $ZnFe_2O_4$ nanoparticles may exist in the grain boundaries but have no large impact due to their small percentage doping.

Figure 4.4 shows the EDX spectra of un-doped CuTl superconductor. The energy dispersive X-ray analysis (EDX) graph of host superconducting matrix CuTl-1223 clearly shows the presence of elements in a sample according to composition with small amount of impurities such as Ni and Fe.

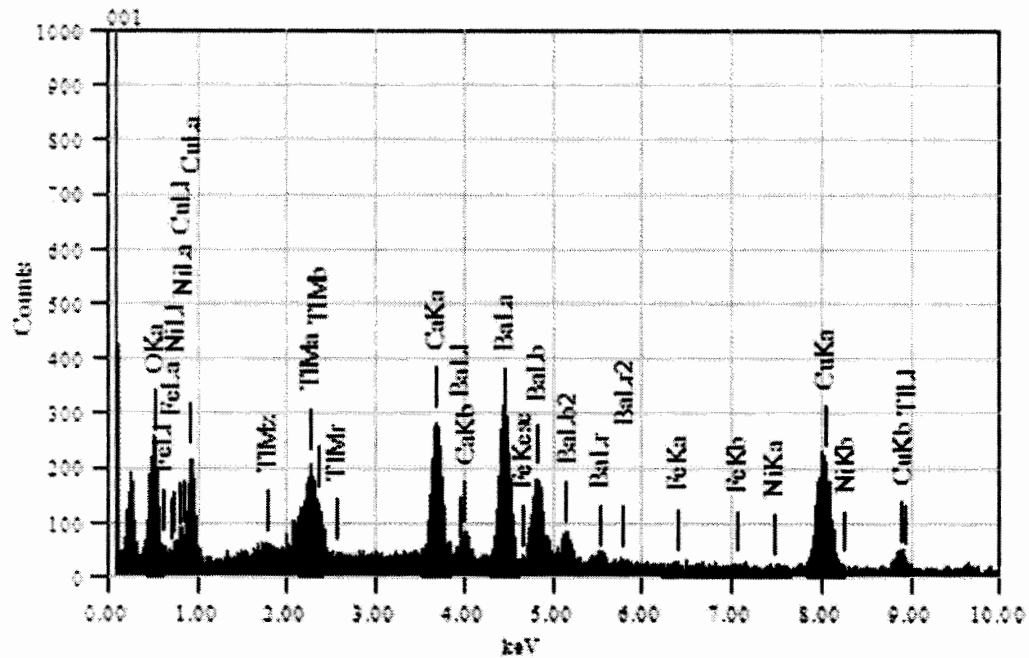


Fig. 4.4: EDX graph of $Cu_{0.5}Tl_{0.5}Ba_2Ca_2Cu_3O_{10-\delta}$ superconductor.

Table 4.1 shows the elemental composition of CuTl superconductor and it shows CuTl-1223 as major phase with small impurities of Ni and Fe with mass %age 0.59 and 0.23, respectively.

Element	keV	Mass%	Error%	Atom%
O K	0.525	11.65	0.68	40.79
Ca K	3.690	8.10	0.55	11.32
Fe K	6.398	0.23	1.21	0.23
Ni K	7.471	0.59	1.81	0.56
Cu K	8.040	33.59	2.37	29.60
Ba L	4.464	36.89	1.64	15.04
Tl M	2.261	8.94	1.70	2.45
Total		100.00		100.00

Table. 4.1:Elements quantitative analysis of EDX presented in Fig. 4.4.

4.3 Fourier transforms infrared spectroscopy (FTIR)

The FTIR spectrum of $ZnFe_2O_4$ nanoparticles in the far-infrared range (400-650 cm^{-1}) is shown in the Fig. 4.5. The band at 420 cm^{-1} is due to the vibration of the chemical $O-M_{Oct}-O$ bond at octahedron position and the band at 546 cm^{-1} is obtained due to the vibration of the chemical bond $O-M_{tet}-O$ at position of the tetrahedron, respectively. The presence of these absorption bands indicates the formation of zinc ferrite spinel structure.

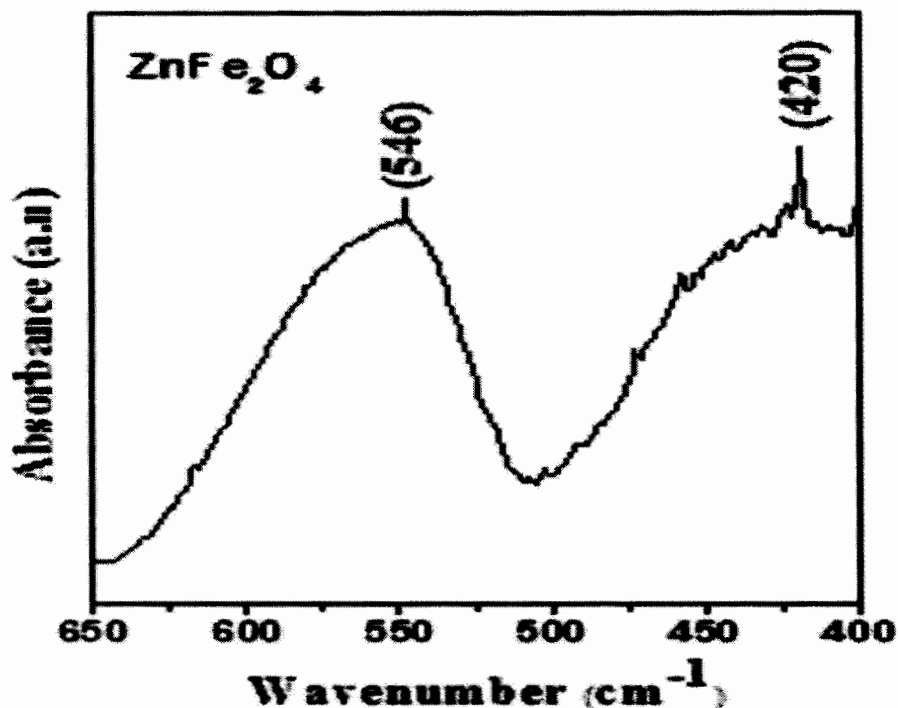
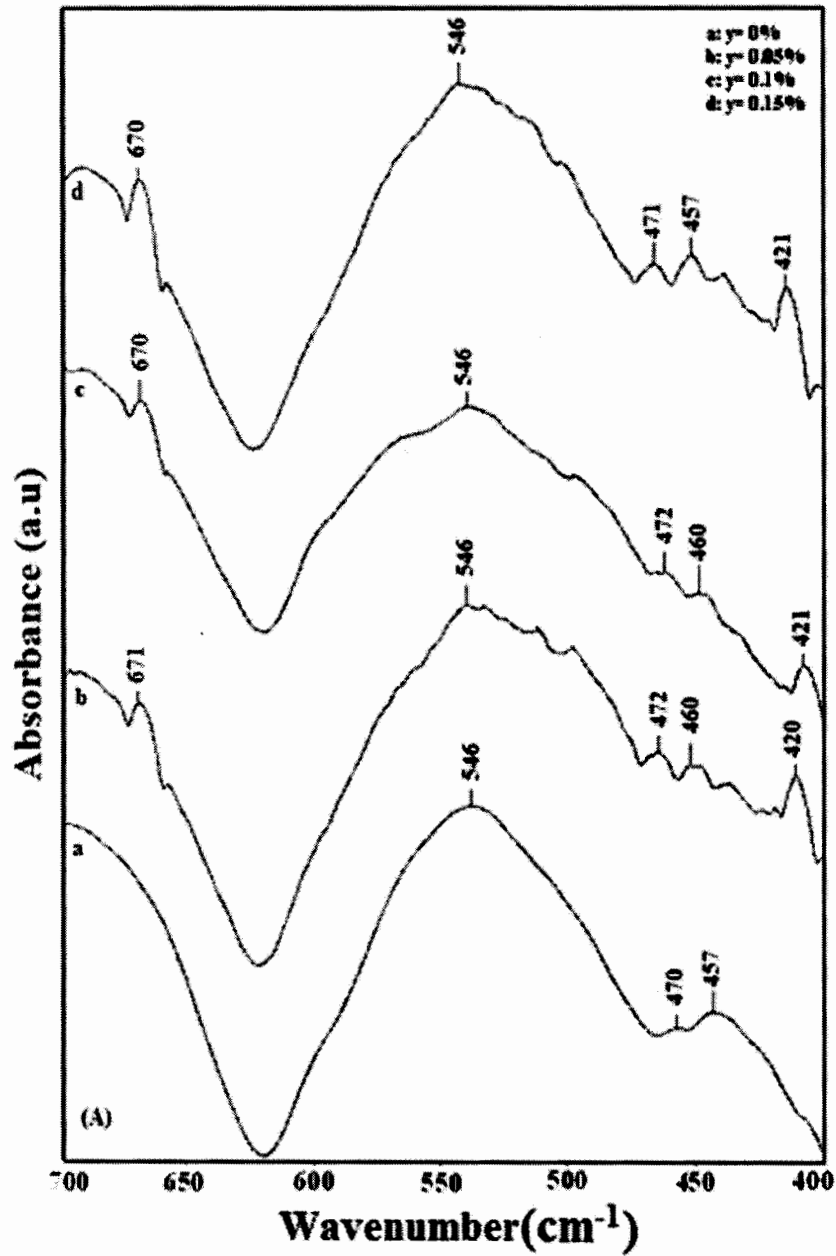


Fig. 4.5: FTIR spectrum of $ZnFe_2O_4$ nanoparticles.

The FTIR absorption spectra of $(ZnFe_2O_4)_y / (Cu_{0.5}Tl_{0.5})Ba_2Ca_2Cu_3O_{10-\delta}$ composites ($y = 0, 0.05, 0.1, 0.15, 0.2, 0.25, 0.5, 1$ and 2%) in the far-infrared range $400-700\text{ cm}^{-1}$ are shown in the Fig. 4.6 (A, B). The FTIR absorption spectrum of the superconductor exhibits the different oxygen atoms vibration in unit cell. The bands in the range from $400-540\text{ cm}^{-1}$ are related to the apical oxygen atoms. In CuO_2 planar oxygen atoms range around $540-600\text{ cm}^{-1}$ and O_8 atoms of charge reservoir layer range is around $670-700\text{ cm}^{-1}$. The absorption band at 420 cm^{-1} in doped sample represent the presence of $ZnFe_2O_4$ nanoparticles and other Zn ferrite peak at 546 cm^{-1} is merged in the superconductor peak. The ferrite nanoparticles doped sample indicates oxygen atoms vibration modes within the range of $435-670\text{ cm}^{-1}$. The oxygen atoms modes variation in

composite of CuTi-1223 w.r.t wt. % of $ZnFe_2O_4$ nanoparticles substitution does not interfere in the composition and no interaction but may enhance the intergrain coupling.



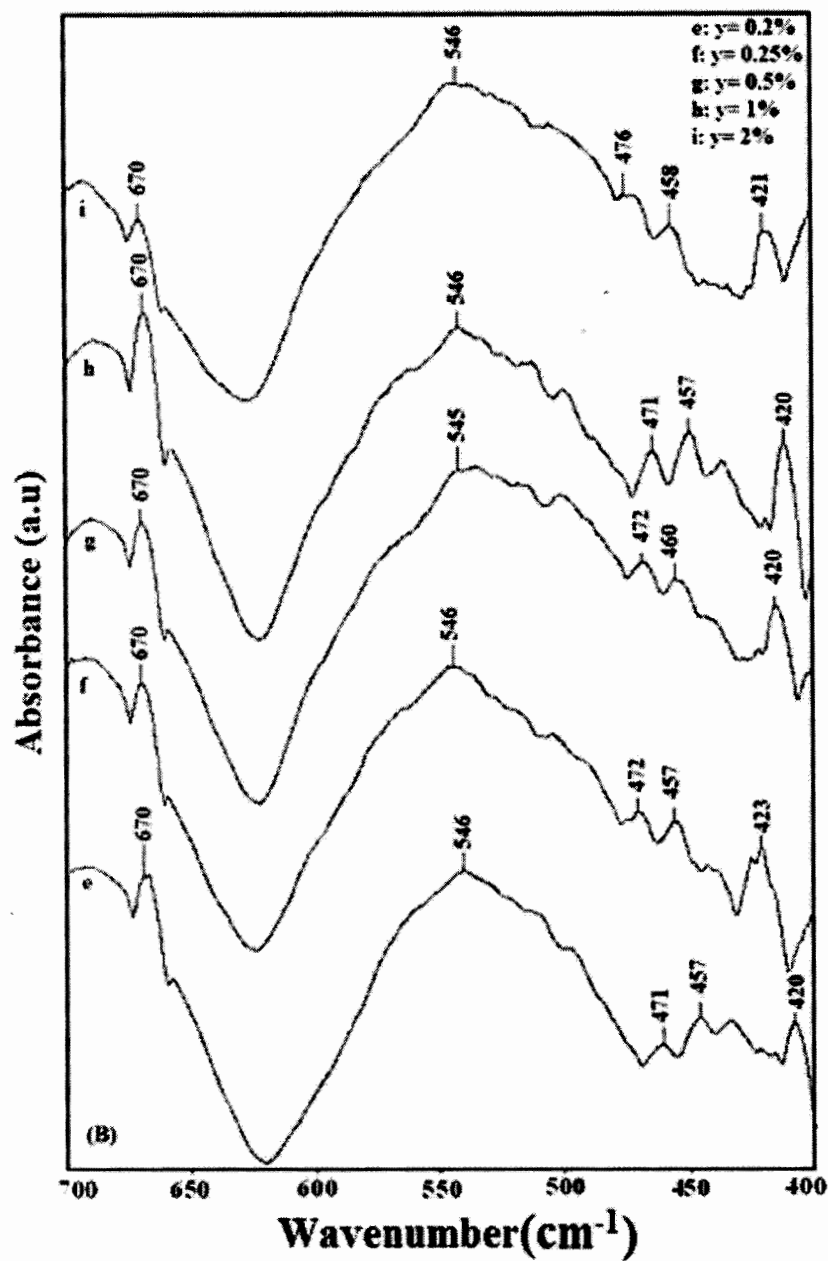


Fig. 4.6: (A) FTIR spectra of $(ZnFe_2O_4)_y/(Cu_{0.5}Ti_{0.5})Ba_2Ca_2Cu_3O_{10-\delta}$ composites a: $y = 0\%$, b: $y = 0.05\%$, c: $y = 0.1\%$, and d: $y = 0.15\%$ superconductors, (B) FTIR spectra of $(ZnFe_2O_4)_y/(Cu_{0.5}Ti_{0.5})Ba_2Ca_2Cu_3O_{10-\delta}$ composites e: $y = 0.2\%$, f: $y = 0.25\%$, g: $y = 0.5\%$, h: $y = 1\%$, and i: $y = 2\%$ superconductors.

4.4 Resistivity measurements

The resistivity measurements of CuTl-1223 samples doped with $(ZnFe_2O_4)_y$ nanoparticles ($y = 0, 0.05, 0.1, 0.15, 0.2, 0.25, 0.5, 1$ and 2%) are shown in the Fig. 4.7 (a, b). The X-Y recorder VP-6424 A from National is used to record the data with the help of origin software and it can be observed from the Fig. 4.7 (a, b) that $T_c (R=0)$ of un-doped CuTl superconductor matrix is 96 K which is depressed after substitution of $ZnFe_2O_4$ nanoparticles with different concentrations such as; $y = 0.05, 0.1, 0.15, 0.2, 0.25, 0.5$ and 1% with T_c 's 93, 92, 91, 94, 95, 80 and 91 K respectively. Composite with 2% nanoparticles doping has T_c below our measurement limit (liquid nitrogen temperature = 77 K), therefore not listed here. The decrease in T_c may signify the trapping of mobile free carriers, lowest porosity and accumulation of nanoparticles in grain boundaries. The variation of resistivity possibly can be occurring due to the reflection of spin charge separation. The poor grain connectivity and alignment is may also be a main reason of T_c suppression in composites.

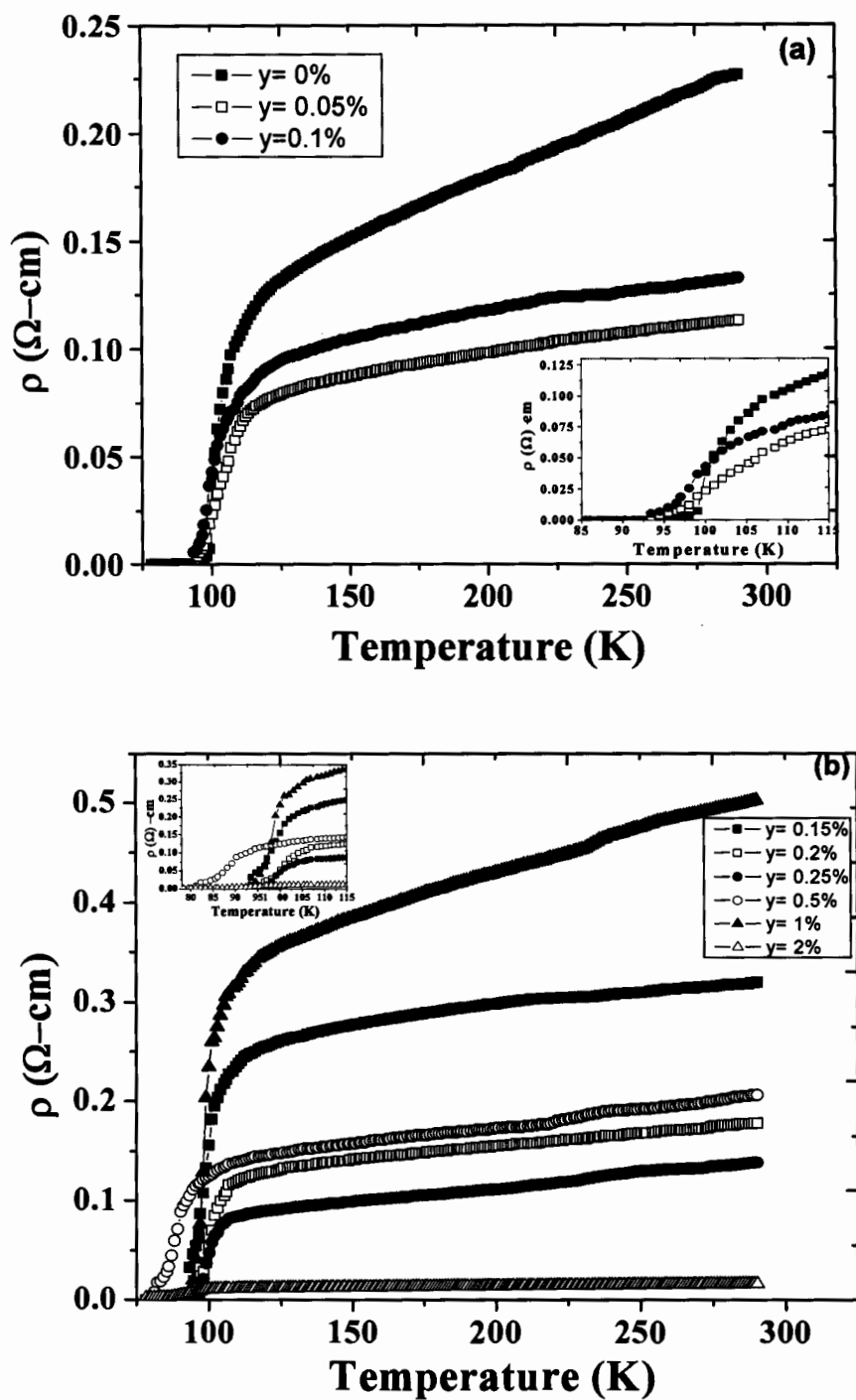


Fig. 4.7: (a) $(\text{ZnFe}_2\text{O}_4)_y / (\text{Cu}_{0.5}\text{Tl}_{0.5})\text{Ba}_2\text{Ca}_2\text{Cu}_3\text{O}_{10-\delta}$ superconductors resistivity vs. temperature measurements of with $y = 0, 0.05$ and 0.1% , (b) Resistivity vs. temperature measurements of $(\text{ZnFe}_2\text{O}_4)_y / (\text{Cu}_{0.5}\text{Tl}_{0.5})\text{Ba}_2\text{Ca}_2\text{Cu}_3\text{O}_{10-\delta}$ superconductors with $y = 0.15, 0.2, 0.25, 0.5, 1$ and 2% .

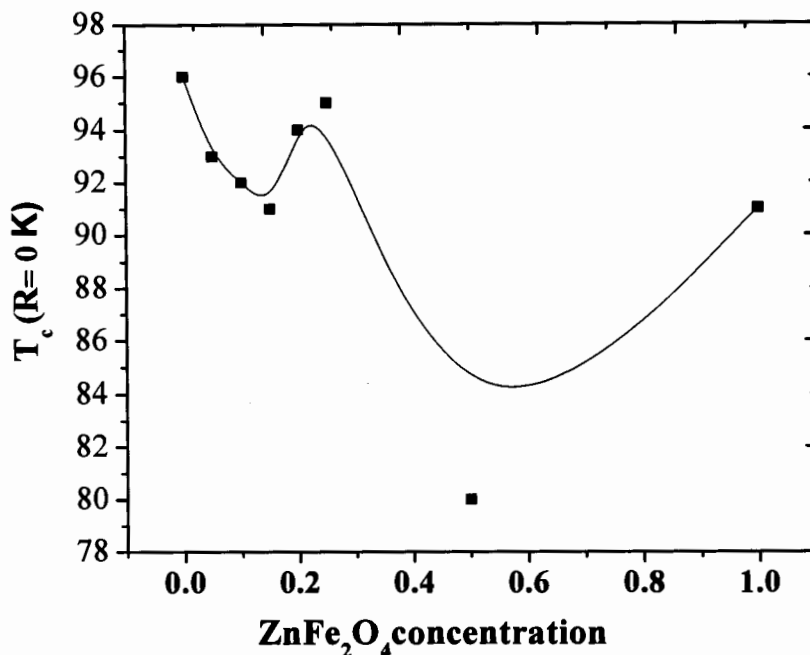


Fig. 4.8: Dependence of critical temperature (T_c) on $ZnFe_2O_4$ nanoparticle concentration.

In Fig. 4.8 solid line just drawn for trend which shows the variation of critical temperature (T_c) with different concentration of $ZnFe_2O_4$ nanoparticles which might be due to disorientation of grain boundaries, impurities phase's composition fluctuation and inhomogeneous distribution of carriers.

4.5 AC susceptibility measurements

The magnetic susceptibility in-phase component (χ') indicates the volume fraction and out-phase component (χ'') shows the energy losses. The temperature dependent AC susceptibility of the composites with $y=0, 0.05$ and 0.1% are shown in Fig. 4.9.

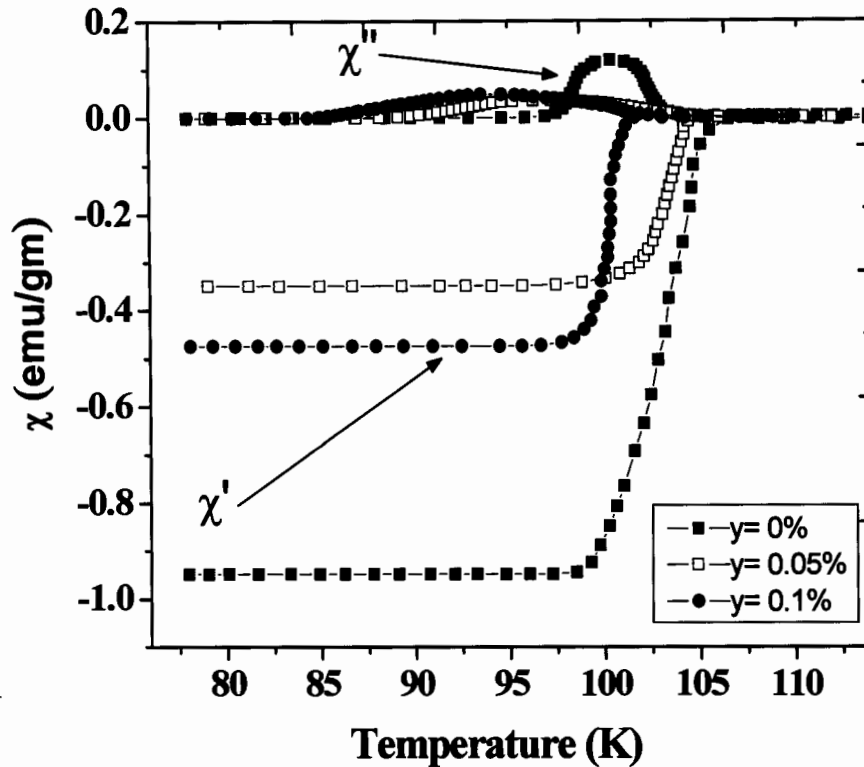


Fig. 4.9: The AC susceptibility vs. temperature measurements of $(ZnFe_2O_4)_y / (Cu_{0.5}Tl_{0.5})Ba_2Ca_2Cu_3O_{10-\delta}$ ($y=0, 0.05$ and 0.1%) superconductors.

The resulting susceptibility curve was plotted on a XY- recorder by using origin software. The out of part (χ'') of AC susceptibility shows a peak behavior which indicates the energy losses at the transition temperature. The broadness of the peak in all presented samples is due to inhomogeneous granular sizes of the CuTl-1223 superconductor. The magnitude of diamagnetism (as evident by in-phase part χ') in $(ZnFe_2O_4)_y$ CuTl-1223 samples is suppressed on increasing the concentration of $ZnFe_2O_4$ nanoparticles which deprive the superconductivity. The decreasing and fluctuation of diamagnetism is possible due to ferrimagnetic behavior of $ZnFe_2O_4$ nanoparticles having a small net

magnetic moment due to disorder and unequal no. of spins on the individual nanoparticle surface.

4.6 Conclusion

We have successfully synthesized the $(ZnFe_2O_4)_y / (Cu_{0.5}Tl_{0.5})Ba_2Ca_2Cu_3O_{10-\delta}$ ($y = 0, 0.05, 0.1, 0.15, 0.2, 0.25, 0.5, 1$ and 2%) nanoparticles/superconductor composites by solid-state reaction method. The structural and physical properties have been examined by X-ray diffraction (XRD), scanning electron microscopy (SEM), Fourier transforms infrared (FTIR) spectroscopy, resistivity, and AC susceptibility techniques. The XRD evaluated structures of nanoparticles and superconductor matrix are spinel and tetragonal, respectively. The size of $ZnFe_2O_4$ nanoparticles is calculated by Debye Scherrer's formula which is 28 nm. According to X-ray diffraction, presence of $ZnFe_2O_4$ nanoparticles in $(Cu_{0.5}Tl_{0.5})Ba_2Ca_2Cu_3O_{10-\delta}$ superconductor has not disturbed the structure of unit cell of host superconductor matrix, which is in accordance with the FTIR measurements. The SEM images prove the granular form of CuTl superconductor matrix. Due to less doping percentage of $ZnFe_2O_4$ nanoparticles they have a minor effect on $Cu_{0.5}Tl_{0.5}Ba_2Ca_2Cu_3O_{10-\delta}$ superconductor grain boundaries. The FTIR spectroscopy confirms the formation of single phase Zn ferrite nanoparticles. The FTIR measurements also confirm the existence of $ZnFe_2O_4$ nanoparticles in composites. Doping of $ZnFe_2O_4$ nanoparticles has decreased the zero resistivity critical temperature [$T_c(R=0)$] and magnitude of diamagnetism. The most likely reason for suppression of superconducting properties due to doping of $ZnFe_2O_4$ nanoparticles in host superconductor matrix is the trapping of mobile free carriers, reflection of spin charge, weak grain connectivity and

porosity. The ferrimagnetic behavior of Zn ferrite nanoparticles causes the depression in magnitude of diamagnetism in AC susceptibility.

References

- [1] C. Kittel, Introduction to Solid State Physics, seventh edition, John Wiley & Sons (2004).
- [2] J. J. Powell, N. Faria, E. Thomas-Mckay, and L. C. Pele, Journal of Autoimmunity 34, J226-J233 (2010).
- [3] S. K. Sahoo, S. Parveen, J. J. Panda, Nanomedicine, 3, 20-31 (2007).
- [4] C. Buzea and K. Robbie, Superconductor. Sci. Technol. 18, R1 (2005).
- [5] K. Shimizu *et al*, Nature 419, 597 (2002).
- [6] J. Nagamatsu *et al* Nature 410, 63 (2001).
- [7] P. W. Philips, Advanced Solid State Physics, Westview Press(2003).
- [8] R. A. Shukor, High Temperature Superconductors: Materials Mechanisms and Applications, AkademiSains, Malaysia (2009).
- [9] W. Meissner, and R. Oschensfeld, Naturwissen Schafttes21, 787 (1933).
- [10] H. K. Onnes, Akad. Van. Wetenschappen (Amsterdam) 14, 113, 818 (1911).
- [11] V. V. Schmidt, The Physics of Superconductors, Nauka Publishers, Moskaue, p: 1 (1982).
- [12] M. S. Vijaya, Materials Science, McGraw-Hill Publishing Company Limited, p: 323, 324 (2003).
- [13] F. and H. London, Proceedings of the Royal Society of London, A149, 71 (1935).
- [14] V. V. Schmidt, The Physics of Superconductors, Nauka Publishers, Moskaue, p: 18, 19 (1982).
- [15] J. Bardeen, L. N. Cooper, and J. R. Schrieffer, Phys. Rev. 108, 1175 (1957).
- [16] H. Ibach and H. Luth, Solid State Physics: An Introduction to Theory and Experiment, Springer-Verleg (1991).
- [17] M. Tinkham, Introduction to Superconductivity, second edition, McGraw-Hill, Inc, New York.
- [18] M. K. Wu, J. R. Ashburn, C. J. Trong, P. H. Hor, R. L. Meng, L. Gao, Z. J. Hung, Y. Q. Wang, and C. W. Chu, Phys. Rev. Lett. 59, 908 (1987).
- [19] C. Michel, M. Hervieu, M. M. Borel, A. Grandin, F. Deslandes, J. Provost, and B. Raveau, Z. Phys. B 68, 421 (1987).

- [20] Y. Muraoka, M. Kikuchi, N. Ohnishi, K. Hiraga, R. Suzuki, N. Kobayashi, and Y. Syono, *Physica C* 204, 65 (1992).
- [21] S. Adachi, H. Yamauchi, S. Tanaka, and N. Mori, *Physica C* 212, 164 (1993).
- [22] Z. Z. Sheng and A. M. Hermann, *Nature* 332, 55 (1988).
- [23] Z. Z. Sheng, A. M. Hermann, A. E. Ali, C. Almasan, J. Estrada, T. Datta, and R. J. Matson, *Phys. Rev. Lett.* 60, 937 (1988).
- [24] W. L. Oslon, M. M. Eddy, T. W. James, R. B. Hammond, G. Gruner, and L. Drabeck, *Appl. Phys. Lett.* 55, 188 (1989).
- [25] H. Ihara, K. Tanaka, Y. Tanaka, A. Iyo, N. Terada, M. Tokumoto, M. Ariyama, I. Hase, A. Sundaresan, N. Hamada, S. Miyashita, K. Tokiwa, and T. Watanabe, *Physica C* 341, 487 (2000).
- [26] S. A. Wolf and V. Z. Kresin, *Journal of superconductivity and novel magnetism* Journal. No 10948, Vol 19 (2006).
- [27] C. Kittel, *Introduction to Solid State Physics* John Wiley & Sons. pp. 273–278 (2004).
- [28] A. A. Abrikosov: *Zh. Eksp. Teor.Fiz.* 32, 1442 English transl.:*Sov. Phys. JETP* 5, 1174 (1957).
- [29] M. A. Omar, *Elementary Solid State Physics*, third edition (2007).
- [30] *Introduction to Superconductivity* second edition, A. C. Rose Innes and E. H. Rhoderick, Pergamon Press, Oxford UK (1969).
- [31] L. Cooper *Physical Review* 104, 1189-1190 (1956).
- [32] U.S. Congress, Office of Technology Assessment, *High-Temperature Superconductivity in Perspective*, OTA-E-440, Washington, DC: U.S. Government Printing Office (April 1990).
- [33] Rohlf, James William, *Modern Physics* 15, Wiley (1994).
- [34] M. A. Omar, *Elementary Solid State Physics*, 3rd Edition, (2007).
- [35] H. Ihara, K. Tokiwa, H. Ozawa, M. Hirabayashi, A. Negishi, H. Matuhata and Y. S. Song, *Jpn. J. Appl. Phys.* 33, L503 (1994).
- [36] Z. Z. Sheng, and A. M. Hermann, *Nature* 332, 138 (1988).

- [37] G. Malandrino, D. S. Richeson, T. J. Marks, D. C. De Groot, J. L. Schindler, and C. R. Kannewurf, *Appl. Phys. Lett.* 58, 182 (1991).
- [38] M. Kikuchi, T. Kajitani, T. Suzuki, S. Nakajima, K. Hiraja, N. Kobayashia, H. Iwasaki, Y. Syono and Y. Muto, *Jpn. J. Appl. Phys.* 28, L382 (1989).
- [39] S. S. P. Parkin, V. Y. Lee, E. M. Engler, A. I. Nazzal, T. C. Huang, G. Gormau, R. Savoy, and R. Beyer, *Phys. Rev. Lett.* 60, 2539 (1988).
- [40] M. Karppinen, H. Yamauchi, Y. Morita, M. Kitabatake, T. Motohashi, R. S. Liu, J. M. Lee, and J. M. Chen, *Journal of Solid State Chemistry* 177, 1037 (2004).
- [41] H. Ihara, *Physica C* 364, 289 (2001).
- [42] K. Tokiwa, H. Aota, C. Kunugi, K. Tanaka, Y. Tanaka, A. Iyo, H. Ihara, and T. Watanabe, *Physica B* 284, 1077 (2000).
- [43] K. Tanaka, A. Iyo, N. Terada, K. Tokiwa, S. Miyashita, Y. Tanaka, T. Tsukamoto, S. K. Agarwal, T. Watanabe, and H. Ihara, *Phys. Rev. B* 63, 064508 (2001).
- [44] T. Shibata, T. Tatsucki, S. Adachi, K. Tanabe, S. Fujihara, and T. Kimura, *Physica C* 353, 200 (2001).
- [45] P. Zoller, J. Glaser, A. Ehmann, C. Schultz, W. Wischert, S. Kemmler-Sack, T. Nissel, and R. P. Huebener, *Z. Phys. B* 96, 505(1995).
- [46] M. Mumtaz, PhD Thesis, Synthesis and characterization of $\text{Cu}_{0.5}\text{Tl}_{0.5}\text{Ba}_2\text{Ca}_{n-1}\text{Cu}_{n-y}\text{Zn}_y\text{O}_{2n+4-\delta}$ ($n = 3, 4$) high temperature superconductors Material Science Laboratory, QAU (2008).
- [47] A. A. Khurram, PhD Thesis, Synthesis and characterization of low anisotropy $\text{Cu}_{1-x}\text{Tl}_x\text{Ba}_2\text{Ca}_2\text{Cu}_3\text{O}_{10-\delta}$ (CuTl-1223) superconductor, Material Science Laboratory, QAU (2006).
- [48] N. Hassan, PhD Thesis, Solid state synthesis and studies of Ni doped superconductor, Material Science Laboratory, QAU (2009).
- [49] M. S. Vijaya, *Materials Science*, McGraw-Hill Publishing Company Limited, p: 352-354 (2003).
- [50] G. Cao, *Nanostructures and Nanomaterials*, Imperial College Press, London(2004).
- [51] N. C. Mueller and B. Nowack, *Elements* 6, 395-400 (2010).
- [52] K. Zamani, *Proc. SPIE* 4608,266 (2002).

- [53] F. Sanchez, K. Sobolev, *Construction and Building Materials* 24, 2060-2071 (2010).
- [54] *Nanotechnology for Dummies*, second edition, John Wiley & Sons (2011).
- [55] R. H. Kodama, *Journal Magn Matter* 200, 359 (1999).
- [56] C. Luna, M. P. Morales, C. J. Serna, and M. Vázquez, *Nanotechnology* 14, 268 (2003).
- [57] *Gold nanoparticles Properties, Characterization and Applications*, Nova Science Publication Incorporated (2010).
- [58] *Surface Effects in Magnetic Nanoparticles*, first edition, edited by D. Fiorani, Springer, New York (2005).
- [59] R. H. Kodama and A. E. Berkowitz, *Phys. Rev. B* 59, 6321 (1999).
- [60] R. H. Kodama, A. E. Berkowitz, J. McNiff E.J., and S. Foner, *Phys. Rev. Lett.* 77, 394 (1996).
- [61] K. Nadeem, T. Traussnig, I. Letofsky-Papst, H. Krenn, U. Brossmann, and R. Würschum, *Journal. Alloys Compounds* 493, 385 (2010).
- [62] C.A. Habertzettl, *Nanotechnology* 13, R9 (2002).
- [63] J.J. Storhoff, R. Elghanian, R.C. Mucic, C.A. Mirkin, and R.L. Letsinger, *Journal: Am. Chem. Soc.* 120, 1959 (1998).
- [64] G.C. Bond, *Catal. Today* 72, 5 (2002).
- [65] T.A. Taton, *Nature Mater* 2, 73 (2003).
- [66] R. F. Service, *Science* 293, 782 (2001).
- [67] T. Hyeon, *The Royal Society of Chemistry*, 927-934 (2003).
- [68] M. S. Vijaya, *Materials Science*, McGraw-Hill Publishing Company Limited, p: 528, 529 (2003).
- [69] M. Daumling, J.C. Grivel, B. Hensel and R. Flukiger, *Physica C* 219, 429 (1994).
- [70] S. A. Sergeenkov, *Physica C* 205, 1-13 (1993).
- [71] N.A. Khan, A.A. Khurram, *Appl. Phys. Lett.* 86, 152502 (2005).
- [72] E. Guilmeau, B. Andrzejewski and J.G. Noudem, *Physica C* 387, 382 (2003).
- [73] A. Ghattas, M. Annabi, M. Zouaoui, F. B. Azzouz and M. B. Salem, *Physica C* 468, 31-38 (2008).

- [74] N. H. Mohammed, A. I. Abou-Aly, I. H. Ibrahim, R. Awad and M. Rekaby, *Journal of Alloys and Compounds* 486, 733-737 (2009).
- [75] M. M. Elokr, R. Awad, A. A. El-Ghany, A.A. Shama and A. A. El-wanis, *Journal Superconductor Nov.Magn* (2010).
- [76] L. Raffott, R. Caciuffoi, D. Rinaldit and F. Liccit, *Supercond. Sci. Technol* 8, 409 (1995).
- [77] G. Subramanyam, Z. Ju, F. Fahmy, P. M. Shand, M. Zhang and P. Boolchand, *Applied Superconductivity* 4 No. 12, 591 (1996).
- [78] X. S. Wu, Z. Q. Mao, J. Lin, W. M. Chen, X. Jin, Xu, Y. H. Zhang, F. M. Pan and S. S. Jiang, *Physica C* 787, 282-287 (1997).
- [79] R. Yanru, L. Hanpeng, L. Mingzhu, T. Qingyun, S. Lihua, L. Zhenjin and M. Xianren, *Physica C* 156, 799 (1998).
- [80] N. M. Hamdan, K. A. Ziq and A. S. Al-Harhi, *Physica C* 314, 125 (1999).
- [81] F. J. Guaita, H. Beltran, E. Cordoncillo, J. B. Carda and P. Escribano, *Journal of the European Ceramic Society* 19, 363-372 (1999).
- [82] C. Liu, A. J. Rondinone and Z. J. Zhang, *Pure Appl. Chem* 72, 37-45 (2000).
- [83] Z. Y. Jia, H. Tang, Z. Q. Yang, Y. T. Xing, Y. Z. Wang and G. W. Qiao, *Physica C* 337, 130 (2000).
- [84] E. Kuzmann, W.T Konig, M.Mair, Z. Homonnay, Z. Klencsar, G. Juhasz, G.Gritzner, *Superconductor. Sci. Technol* 14, 379-385 (2001).
- [85] F. Grasset, N. Labhsetwar, D. Li, D. C. Park, N. Saito, H. Haneda, O. Cador, T. Roisnel, S. Mornet, E. Duguet, J. Portier and J. Etourneau, *Langmuir* 18, 209-216 (2002).
- [86] S. Soltanian, J. Horvat, X. L. Wang, P. Munroe and S. X. Dou, *Physica C* 390, 185 (2003).
- [87] S. Y. Xie, Z. J. Ma, C. F. Wang, S. C. Lin, Z. Y. Jiang, R. B. Huang, and L. S. Zehang, *Journal. Solid State Chem.* 177, 3743 (2004).
- [88] Y. Jia, H. Niu, M. Wu, M. Ning, H. Zhu, and Q. Chen, *Material Research Bulletin* 40, 1623 (2005).
- [89] B. P. Rao and O. F. Caltun, *Journal of Optoelectronics and Advanced Materials* 8, 991-994 (2006).

- [90] C. Yao, Q. Zeng, G. F. Goya, T. Torres, J. Liu, H. Wu, M. Ge, Y. Zeng, Y. Wang and J. Z. Jiang, *Journal. Phys. Chem. C*, 111, 12274-12278 (2007).
- [91] Y. Xu, A. Hu, C. Xu, N. Sakai, I. Hirabayashi and M. Izumi, *Physica C* 468, 1363–1365 (2008).
- [92] S.G. Elsharkawy and R. Awad, *Journal of Alloys and Compounds* 478, 642–647 (2009).
- [93] N. H. Mohammed, A. I. Abou-Aly, I. H. Ibrahim, R. Awad and M. Rekaby, *Journal Superconductor Nov Magn* (2010).
- [94] M. Frabod and M. R. Batvandi, *Physica C* 471, 112 (2011).
- [95] N. A. Khan, A. Saleem and S. T. Hussain, *Journal Superconductor Nov Magn* (2012).
- [96] C. N. R. Rao, *Chemistry of High Temperature Superconductors* (Ed), Singapore: World Scientific (1991).
- [97] C. N. R. Rao, *Phil. Trans. R. Soc. A336*, 595 (1991).
- [98] C. N. R. Rao, and J. Gopalakrishnan, *New Directions in Solid State Chemistry* Cambridge: Cambridge University Press (1989).
- [99] B. D. Cullity, *Elements of X-ray Diffraction*, Addison-Wesley Publishing Company, Inc (1956).
- [100] C. Giacovazzo, *Fundamentals of Crystallography*, second edition, Oxford science publications (2002).
- [101] B. E. Warren, *X-ray Diffraction*, General publishing company (1969).
- [102] L. Alexander and H. P. Klug, *Journal. Appl. Physics* **21**, 126 (1950).
- [103] S. Amelinckx, D. V. Dyck, J. V. Landuyt and G. V. Tendeloo, *Handbook of Microscopy Methods II* (1997).
- [104] H. Ibach and H. Luth, *Solid State Physics: An Introduction to Theory and Experiment*, Springer-Verlag (1991).
- [105] M. Nikolo Am. *Journal. Physics* 63, 57-65 (1995).
- [106] M. I. Youssif, A. A. Bahgat and I. A. Ali, *Egypt. Journal. Sol.*, Vol 23 (2000).
- [107] H. Ihara, A. Iyo, K. Tokiwa, K. Ishida, N. Terada, M. Tokumotu, Y. Sekita, T. Tsukamoto, T. Watanabe, and M. Umeda, *Physica C* 282-287 (1997).

- [108] H. Yamauchi, M. Karppinen, and S. Tanaka, *Physica C* 263, 146-150 (1996).
- [109] V. Bartunek and O. Smrckova, *Ceramics-Silikaty* 54, 133-138 (2010).
- [110] S. X. Dou, S. Soltanian, J. Horvat, X. L. Wang, P. Munroe, S. H. Zhou, M. Ionescu, H. K. Liu, and M. Tomsic, *Applied Physics Letters* 81, 18 (2002).
- [111] M. Annabi, A. M_chirgui, F. Ben Azzouz, M. Zouaoui, and M. Ben Salem, *Physica C* 405, 25-33 (2004).
- [112] S. X. Dou, S. Soltanian, Y. Zhau, E. Getin, Z. Chen, O. Shcherbakoba and J. Horvat, *Superconductor. Sci. Technology*, 18, 710-715 (2005).
- [113] I. E. Agranovski, A. Y. Iiyushechkin, I. S. Altman, T. E. Bostrom and M. Choi, *Physica C* 434, 115-120 (2006).
- [114] C. Xu, A. Hu, M. Ichihara, N. Sakai, I. Hirabayashi and M. Izumi *Physica C* 460-462, 1341-1342 (2007).
- [115] R. Awad, *Superconductor Nov Magn* 21, 461-466 (2008).
- [116] M. Mumtaz and N. A. Khan, *Physics.Scr.* 80 (2009).
- [117] B. A. Albiss, I. M. Obaidat, M. Gharaibeh, H. Ghamlouche and S. M. Obeidat, *Solid State Communications* 150, 1542-1547 (2010).

